Developing an impedimetric glucose sensor using multi-layer molecularly imprinting technique

by

Koorosh Abbaspour

B.Sc., University of Science and Technology, 2017

M.Sc., University of Tehran, 2021

A THESIS SUBMITTED IN PARTIAL FULFILLMENT OF

THE REQUIREMENTS FOR THE DEGREE OF

MASTER OF APPLIED SCIENCE

in

THE FACULTY OF GRADUATE STUDIES

(Department of Mechanical Engineering)

THE UNIVERSITY OF VICTORIA

We acknowledge and respect the Lək̓ʷəŋən (Songhees and Xʷsepsəm/ Esquimalt) Peoples on whose territory the university stands, and the Lək̓ʷəŋən and W̱SÁNEĆ Peoples whose historical relationships with the land continue to this day

Supervisory Committee

Developing an impedimetric glucose sensor using multi-layer molecularly imprinting technique

Koorosh Abbaspour

B.Sc., University of Science and Technology, 2017

M.Sc., University of Tehran, 2021

Supervisory Committee:

Mina Hoorfar, Department of Mechanical Engineering
Supervisor

Jason Keonhag Lee, Department of Mechanical Engineering
Member

Makhsud Saidaminov, Department of Chemistry and Electrical and Computer Engineering
Member

Abstract

A sensitive and cost-effective measurement of glucose has always been a priority in clinical and quality control arena. In this article, molecularly imprinted and non-imprinted polymer (MIP & NIP) based on conducting polymers and functionalized composites was suggested to achieve repeatable and stable determination of glucose in POC analyses. Glucose was introduced into the imprinted layer composed of polypyrrole (PPy) along with (APBA), which was formed on the carboxylayed multiwalled carbon nanotubes (COO-MWCNT) as the step to immobilize glucose. Further polymerization of an imprinting layer for glucose, in a basic medium, was performed to cage the glucose molecule. A layer-by-layer analysis of the sensor was performed with electrochemical and surface analyzing methods. Also, both NIP and MIP were characterized before and after the glucose removal by phosphate buffer. The glucose rebinding to form gluco-boronate ester in sensor was tested using impedance technique and a linear range between 1 µM and 20 µM with the detection limit of 6 µM was achieved. The reusability and stability of the imprinted sensor were determined to be 10 times and 96% of the beginning current was maintained after 15 days. In overall, such a sensor demonstrates promising future for developing cheap, reusable and non-invasive glucose sensors.

Keywords: Glucose, Molecularly imprinted polymer, Carboxylated multi-walled carbon nanotubes, Impedance measurement, Non-invasive glucose sensor

Table of Contents

Supervisory Committee ***1***

Abstract ***iii***

Table of Contents ***iv***

List of Figures ***vii***

Lay Summary ***xi***

Preface ***xii***

Acknowledgements ***xiii***

Dedication ***xiv***

Chapter 2 Introduction ***1***

Chapter 3 Literature Review *Error! Bookmark not defined.*

2-1. Glucose sensing in diabetic patients **9**

2-2. Different strategies for sensing Glucose **11**

2.2.1- Glucose detection by enzymatic Methods 11

2.2.2-Glucose detection by Non-Enzymatic Methods 13

2.2.3-Background knowledge for non-enzymatic glucose electrochemical sensors 14

2.2.4- Direct glucose oxidation via metallic redox centers 17

2.2.5- Nonfaradaic detection via association with glucose 19

2-2-6. Molecularly imprinted polymers-based electrochemical biosensors 23

2.2.6.2- Electrosynthesized MIP-based sensors for detection of saccharides 25

2-4. Motivation and Objective **29**

2-5. Thesis Outline **29**

Chapter 4 Methodology ***29***

3-1. Materials and Methods **30**

3-2. Synthesis of MWCNT-COOH **31**

3-2-1. Pirranha-treated MWCNTs 31

3.2.2- Hydrothermal treatment 31

3-2-3. Preparation of APBA-MWCNT nanocomposites 32

3-3-Electrochemical technique for developing biomimetic sensors **33**

3-3-1. Electrochemical cell 34
3-3-2. Electrochemical measurements 35
3-3-3-Characterization techniques 43

Chapter 5 *45*

Results and Discussion *45*

4-1. Steps to fabricating glucose sensor **46**

4-1-1- Electro-cleaning of the electrode 46
4-1-2- Electropolymerization of conductive polymer **Error! Bookmark not defined.**
4-1-4- Drop casting the template molecule 48
4-1-5- Formation of imprinting layer 48
4-1-6- Washing step 49

4-2. Material Characterizations **51**

4-2-1- Scanning electron microscopy (FE-SEM)/ Energy dispersive X-ray (EDX) 51
4-2-2- Raman spectroscopy 56

4-3- Electrochemical Characterizations **57**

4-3-1- CV and EIS characterizations 57

4-4- Molecularly imprinted sensor platform **60**

4-4-1- Developing glucose-responsive system 60
4-4-2- Characterization of MIP and NIP sensors 62
4-4-3- Analytical performance of MIP Sensor 66
4-4-4- Sensor stability and reusability 68

Chapter 6 *73*

Conclusion & Future work *73*

5-1. Summary **74**

5.2- Future Work **75**

Chapter 7 *78*

Bibliography *78*

List of Figures

Figure 1-1 Schematic for diabetes management, non-invasive biofluids, alternatives to blood glucose assays, and examples of notable wearable platforms used for continuous, non-invasive glucose monitoring from these biofluids [5] 3

Figure 1-2 Different lab-based techniques for diagnosis of diabetes 4

Figure 1-3 Different fundamental factors in gas sensing application: sensitivity, selectivity, stability, operating time, limit of detection and power consumption [8] 5

Figure 1-4 Schematic representation of generic synthesis and rebinding of molecularly imprinted polymers [12] 6

Figure 2-1 Schematic diagram of the surface-imprinted polyscopoletin nanofilm and its use for protein detection [20] 11

Figure 2-2 Schematic representation of the principles of first-, second-, and third-generation glucose sensors 12

Figure 2-3 (a) Molecular structures of various D-glucose isomers (b) Overall process of glucose oxidation. The reaction proceeds from D-glucose into D-glucono-d-lactone via slow hydrogen abstraction and oxidation, followed by fast hydrolysis into D-gluconic acid [28] 15

Figure 2-4 (a) The chemisorption mechanism of glucose oxidation. (b) Incipient hydrous oxide/adatom mediator model[39] 18

Figure 2-5 (a) The possible equilibria of bor(on)ic acid and diols in aqueous solution. The boronic and related compounds easily form diesters 1,2- and 1,3-diols.[54] (b) Schematic representation of molecular imprinting by non-covalent interactions between the analyte and functional monomers. The molecularly-imprinted polymer selectively rebinds to molecules matching the imprinted binding sites, analogous to the binding sites of biomolecules such as enzymes and receptors [53] 22

Figure 2-6 The surface imprinting strategy for the synthesis of a protein-MIP layer on a conducting surface using the electropolymerization approach. The strategy consists of (A) covalent immobilization of a target protein via a cleavable linker to a conducting surface; (B) electropolymerization of a monomer with careful control of the thickness of the growing polymer to exclude protein entrapment; (C) cleavage of the linker to facilitate protein removal; and (D) formation of MIP with protein-selective binding sites located on the polymer surface [49]. 24

Figure 2-7 A surface imprinting approach combines colloidal crystal templating with electropolymerization to fabricate an inverse opal structure with molecular imprints of a protein (e.g., hCG) on the surface. The approach includes the following steps: (A) fabrication of a colloidal crystal template of SiO2 NPs; (B) immobilization of target protein (hCG) on the surface of NPs; (C) derivatization of protein with functional monomers (bithiophene); (D) electrodeposition of poly(2,3′-bithophene) film; (E) removal of NPs and the protein from the polymer, resulting in a polymeric inverse opal material with molecular cavities on the inner side of the pore wall [55] 25

Figure 2-8 Examples of using “gating effect” for indirect electrochemical detection of the analyte at the MIP-based electrode and the corresponding current potential signals [56] 26

Figure 2-9 Graphical depiction of the constructed EP-imprinted biosensor preparation[58] .. 28

Figure 3-1 The protocol for Synthesizing surface-oxidized MWCNTs 32

The oxidized MWCNTs were dispersed in ultrapure water to achieve a concentration of 1 mg/mL. While stirring rapidly, EDC (0.05 g) was added quickly, and the mixture was continuously stirred at room temperature for 1 hour. Next, NHS (0.1 g) was added to the suspension. Subsequently, APBA (0.05 g) was added, and the solution was stirred overnight at room temperature. The APBA-functionalized MWCNTs were then rinsed with ultrapure water and re dispersed in ultrapure water at a concentration of 1 mg/mL as illustrated in Figure 3-2. At last, a grey solution of APBA-MWCNT is resulted. 32

Figure 3-2 The electrochemical setup for sensing glucose 34

Figure 3-3 Our three-electrode system device 35

Figure 3-4 Typical cyclic voltammogram of 0.1 mM K3Fe (CN)6 in 1.0 M NaN03 on bare platinum 36

Figure 3-5 The differential pulse voltammetry mechanism [60] 39

Figure 3-6 Typical response of a differential pulse voltammogram [60] 40

Figure 3-7 Square wave voltammetry waveform [60] 41

Figure 3-8 EIS of a Randles circuit including a Warburg element in a schematic Bode and Nyquist plot [61] 42

Figure 3-9 Different light scattering modes: Rayleigh, Stokes, and anti-Stokes scattering [62] 44

Figure 4-1 Electro-washing of SPCE 46

Figure 4-2 (a) current profile of electropolymerization at constant potential (b) Charge transfer profile of electropolymerization at constant potential 47

Figure 4-3 (a) Electropolymerization of PPy/ APBA imprinting layer in PBS (pH=13) under optimized conditions (b) Schematics of fabricated sensor with and without presence of glucose49

Figure 4-4 Sensor Optimization experiments for glucose recognition after the formation of imprinting layer: (a) scan rate of polymer deposition (b) number of cycles for imprinting layer electrodeposition (c) APBA concentration (d) Ratio of imprinting polymers (e) Ratio of Template/Monomer (f) Immersion time for glucose binding. 50

Figure 4-5 The sequential steps for fabricating Glucose MIP Sensor 51

Figure 4-6 SEM images of multi-step Glucose sensor fabrication at × 11000 magnification. (a) Electrowashed electrode (b) Elecropolymerized pyrrole layer deposition (c) MWCNT drop-casting (d) APBA-MWCNT drop-casting (e) Glu immobilized onto APBA-MWCNT layer..... 52

Figure 4-7 characterization of the sensor. EDS mappings for carbon (C), oxygen (O), nitrogen (N), chloride (Cl) of the sensor at different stages of preparation and the corresponding EDS spectra (a-d). (Bare carbon tri-electrode: Fig. (a),(f); after Pyrrol polymerization: Fig. (b), (g); after MWCNT deposition: Fig. (c), (h); deposition of MWCNT-APBA: Fig. (d), (i)..... 54

Figure 4-8 SEM characterization of film thickness (a) bare electrode (b) PPy-coated (8.28±0.5 μm) (c) Final composite layer (7.93±0.7μm). the film thickness were estimated by

focusing on the cross-section of polymer film layer position on top of an angular stub. without gold coating. 55

Figure 4-9 (a) Raman spectra of (a) layer-by-layer film modifications (b) MWCNT and MWCNT-COOH (c) 0.1 M glucose in dionized water 57

Figure 4-10 (a) CV characterization of developed sensor from Acid-treated to APBA/f-MWCNT modification (b) Electrochemical impedance spectra at Acid-treated, PPy/SPCE, f-MWCNT/SPCE and APBA/f-MWCNT/SPCE. Measurement were taken at room temperature with 2.5mM $Fe(CN)_6^{3-/4-}$(1:1) 58

Figure 4-11 Cyclic voltammograms: the bare (a) and functionalized (b) SPCE under different scan rates (0.01->0.15) in 0.1M KCl+ 5 mM $Fe(CN)_6^{3-/4-}$ (c) the relationship between the anodic/cathodic current peaks of the redox mediator at the electrodes ...and the square root of the corresponding scan rates. 60

Figure 4-12 (a) finding optimum pH for glucose binding (b) Electrochemical Impedance spectra at APBA-MWCNTs/Ppy/SPCE and Glucose-bound/APBA-MWCNT/Ppy/SPCE (c) Differential pulse voltammetry of APBA-MWCNTs/Ppy/SPCE and Glucose-bound/APBA-MWCNT/Ppy/SPCE(Glucose concentration:10µM). Optimization for pH was done at 0.01 M PBS; EIS and DPV experiments were conducted in 2.5 mM $Fe(CN)_6^{3-/4-}$. 61

Figure 4-13 CV and EIS analysis of MIP and NIP (a,b) before and (c,d) after PBS washing. 63

Figure 4-14 (a) Illustration of template removal mechanism (b) Effective elution time of glucose in PBS (pH=3.5) (c) SEM images of MIP and NIP before and after the elution. 64

Figure 4-15 (a) Electrochemistry of glucose in -1v_1.5v range for 100 mvs and 2 cycles in PBS at pH=8 (b) Chronoamperometry measurements recorded at applied potential of 1.1 v for MIP in 0.1 mol L^{-1} PBS (pH 8) with different concentrations of glucose from 0.1 to 1 mol L^{-1}. 65

Figure 4-16 Square wave voltammograms recorded for the concentration dependent detection of glucose in PBS (pH=8). SWV measurements were conducted at room temperature with 5mM Fe(CN)63-/4- in 0.1 KCl 67

Figure 4-17 Electrochemical impedance spectra obtained for MIP(c&d) and NIP(a&b) sensor for concentration dependant detection of glucose in PBS (pH=8). EIS experiments were conducted in 0.1 M PBS containing 5 mM $Fe(CN)_6^{3-/4-}$ 68

Figure 4-18 Interference study of ascorbic acid 70

Figure 4-19 (a) Stability of Sandwich-MIP sensor over a period of 30 days (b) peak current of glucose after glucose elution and rebinding from 1^{st} time to 10^{st} time. Glucose concentration: 10µM 71

List of Tables

Table 4-1 Comparisons of the sensing performance for the MIP-based electrochemical sensors for glucose detection. 72

Lay Summary

In this project, a novel sandwich-type MIP sensor is developed for glucose detection. The sensor demonstrates high sensitivity, stability and appreciable reusability offering potential applications in a point-of-care systems. The successful employment of the sandwich-type sensors contributes to the advancement of non-invasive sensor development.

Preface

The research presented in this thesis is the original work performed by the author. This thesis was supervised by Dr. Mina Hoorfar at the Microfluidics and Nanotechnology (MiNa) laboratory in the Faculty of Mechanical Engineering at the University of Victoria.

Acknowledgements

I would like to express my gratitude to Dr. Mina Hoorfar, my supervisor, Dr. Somayeh Fardindoost, our postdoctoral fellow, **Emily Earl** and Jacobe Stachowski, our lab engineers, and all graduate students in our team for providing me with excellent support throughout this journey

Dedication

This dissertation is dedicated to my Mom, Dad, and my siblings whom their unlimited love, support, and encouragement nourished my soul and inspired me to pursue my dreams. Also, to my lovely wife, without whom I would not have been able to accomplish my research achievements.

1. Introduction

Diabetes mellitus is a chronic metabolic disorder characterized by high blood glucose levels due to either insufficient insulin production or the body's inability to effectively use insulin. There are several types of diabetes, with Type 1 diabetes resulting from autoimmune destruction of insulin-producing beta cells in the pancreas, and Type 2 diabetes being associated with insulin resistance and often linked to obesity and lifestyle factors[1]. The global prevalence of diabetes is alarming, with approximately 450 million people affected, and projections suggest this number could rise to 600 million by 2030 [1]. While the numbers are getting increasingly high, it is important to effectively manage diabetes mellitus to improve the quality of life. Among the several strategies that have been reported for diabetes mellitus management, controlling the temporal glucose profile can suggest better management of the glycemic conditions [2]. Non-invasive glucose sensors are emerging technologies that allow for the monitoring of glucose levels without the need for blood samples. These sensors utilize various biofluids such as sweat, saliva, interstitial fluid (ISF), and tears to measure glucose concentrations, making them a more comfortable alternative to traditional fingerprick blood tests (Figure 1-1). Electrochemical sensors emerge as a promising technology for glucose monitoring as they offer advantages that enhance diabetes management compared to other techniques. Electrochemical sensor provides quick detection of glucose levels, which means they are designed so that they will be highly selective to glucose and minimize interference from other substances in the biological fluid. Additionally, the electrochemical platforms can utilize alternative body fluids such s sweat, saliva or ISF instead of blood. This non-invasive approach significantly reduces discomfort associated with traditional finger-prick methods. These sensors are also capable of providing continuous glucose monitoring (CGM), which is essential for tracking dynamic changes in glucose levels throughout the day (Figure 1-2).

Glucose sensors utilizing the electrochemical properties of glucose have undergone continuous development over the past several decades, incorporating various technologies and detection mechanisms. First-generation sensors rely on glucose oxidase to catalyze the oxidation of glucose, producing hydrogen peroxide as a byproduct. Detection in these sensors is achieved by measuring the current generated from the oxidation of hydrogen peroxide at the electrode surface. However, their performance is highly dependent on the presence of oxygen in the environment, which can limit their effectiveness in low-oxygen conditions. Second-generation electrochemical sensors also employ glucose oxidase but utilize synthetic redox mediators, such as ferrocene, instead of oxygen. These mediators facilitate electron transfer between the enzyme and the electrode, enabling glucose detection at lower potentials [3].

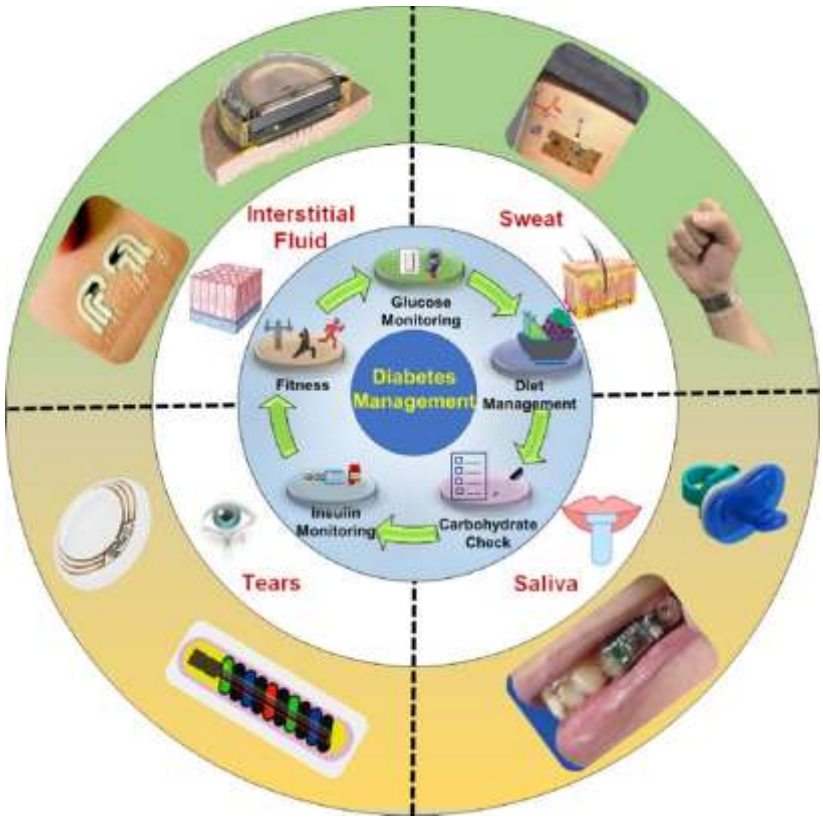

Figure 1-1 Schematic for diabetes management, non-invasive biofluids, alternatives to blood glucose assays, and examples of notable wearable platforms used for continuous, non-invasive glucose monitoring from these biofluids [4]

Furthermore, glucose dehydrogenase (GDH)-based sensors have been developed, which operate independently of oxygen, offering a significant advantage over GOx-based sensors in oxygen-deprived environments [3].

The reaction produces NADH, which is detectable through electrochemical methods. However, detecting NADH usually requires higher electrode potentials, which may introduce challenges such as electrode fouling and interference from other substances. Non-enzymatic electrochemical sensors represent an alternative class of glucose sensors, where glucose is directly oxidized at the electrode surface. Numerous anti-interference strategies are also employed to prevent extraneous substances from impacting the sensor's accuracy. These strategies are designed to minimize the influence of coexisting electroactive species that may interfere with glucose detection [3].

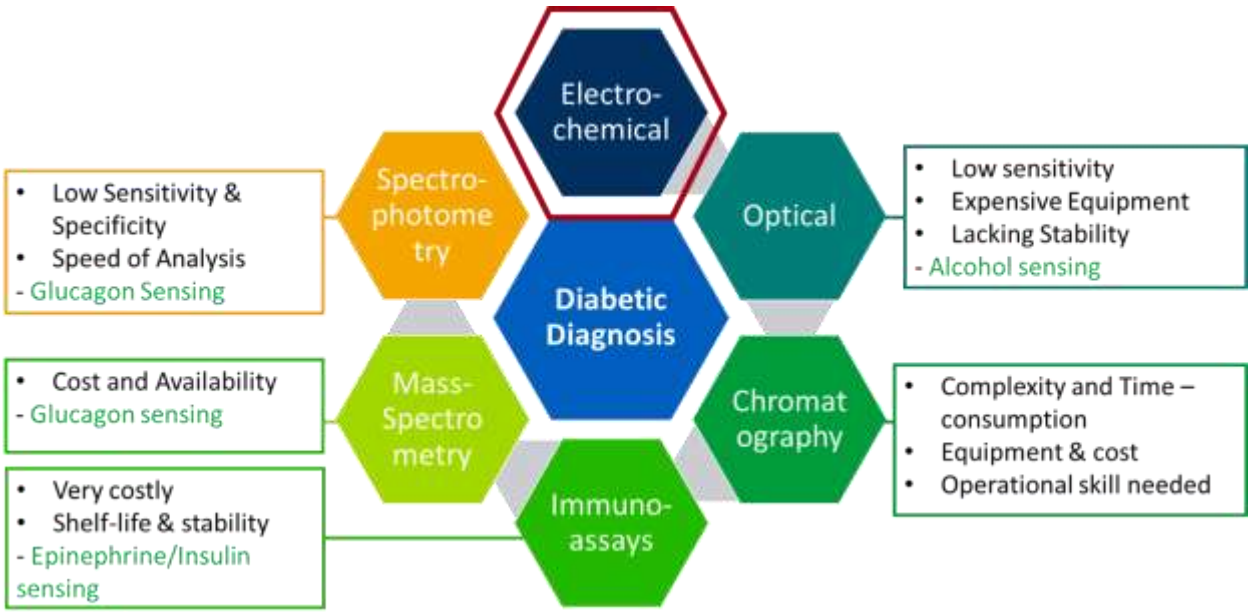

Figure 1-2 Different lab-based techniques for diagnosis of diabetes

In this research, a non-enzymatic electrochemical glucose sensor has been developed. Additionally, an anti-interference strategy has been put in place to ensure the selectivity of sensor toward glucose. Since the primary goal of a glucose sensor is to provide accurate and reliable data

in a sample, whether it is blood, plasma or interstitial fluid, assessing characteristics like selectivity, sensitivity and stability ensures the sensor can detect and measure glucose correctly without interference from other substances. Inaccurate readings could lead to wrong medical or industrial decisions. In glucose sensing, different fundamental factors are of utmost importance: sensitivity, selectivity, stability, operating time, limit of detection and power consumption as shown in (Figure 1-3). Sensitivity is the ratio of a sensor's response change to the change in analyte concentration. Highly sensitive sensors detect a wide range, including low concentrations, while low-sensitivity sensors are limited to higher concentrations. Selectivity refers to the sensor's ability to detect a specific target while distinguishing it from other substances. Stability reflects the sensor's capacity to maintain performance over time, despite environmental changes. Operating time includes the response time to 90% saturation and the recovery time to 60% baseline. The limit of detection is the lowest concentration detectable, and power consumption refers to the external energy required for detection [5-8].

Figure 1-3 Different fundamental factors in gas sensing application: sensitivity, selectivity, stability, operating time, limit of detection and power consumption [7]

Among the various methods used to ensure stability and selectivity, molecularly imprinted polymers known as MIPs can offer increased selectivity together with improved selectively. MIPs are synthetic materials designed with specific recognition sites that mimic natural binding sites for target molecules, such as glucose or other analytes. In summary, molecularly imprinted polymers capture template molecules by creating specific recognition sites within a polymer matrix that are

complementary in shape, size, and functional groups to the target molecule. The process begins with the template molecule interacting with functional monomers via non-covalent or covalent bonds in a pre-polymerization solution. These monomers form a structured arrangement around the template. During polymerization, cross-linking agents solidify the structure, creating rigid binding sites. Once the template is removed, these sites remain and are perfectly suited to selectively rebinding the template or similar molecules [9-11]. The selective binding occurs through interactions such as hydrogen bonding or electrostatic forces. By integrating MIPs into the sensor design, the sensor's selectivity can be significantly improved, allowing for more precise detection of specific molecules in complex environments (Figure 1-4). Additionally, MIPs provide increased stability, as they are resistant to harsh conditions like temperature and pH changes, and they do not degrade as quickly as biological recognition elements. This makes MIP-based electrochemical sensors particularly attractive for long-term and continuous monitoring applications.

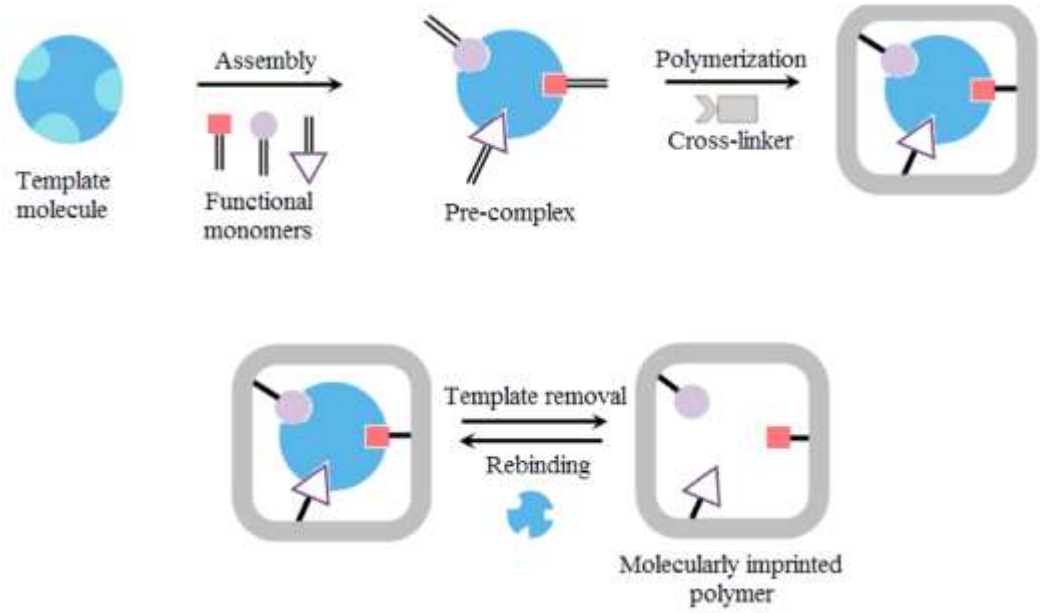

Figure 1-4 Schematic representation of generic synthesis and rebinding of molecularly imprinted polymers [11]

The electrochemical method relies on the oxidation or reduction of an electrically activated compound, which may either be a reaction product or a redox couple functioning as a mediator between the analyte and the electrode. Various techniques, such as amperometry, conductometry, potentiometry, and impedancemetry, can be used to record and process the analytical signals in these electrochemical biosensors. Among these, amperometric biosensors are the most widely utilized. However, a key limitation of this approach is the application of high potentials to the biosensor, which can lead to a gradual decrease in activity and, ultimately, biosensor degradation. To overcome this limitation while preserving high sensitivity to glucose concentration, alternative methods of signal registration and analysis, such as electrochemical impedance spectroscopy (EIS), can be employed. A key advantage of the EIS method is its non-destructive effect on the electrochemical system. EIS allows the recording of an electrochemical response by applying an alternating current with a small amplitude to the electrode. Recently, the use of EIS has expanded in the study of electrochemical properties of biological systems. In these studies, EIS has been applied to characterize various stages of electrode preparation, while the current strength measured by voltammetry serves as the analytical signal [12]. In this research, EIS was used to demonstrate the variation in charge transfer resistance with increasing glucose concentrations. Additionally, the EIS method provides more precise data compared to traditional amperometric sensors. Moreover, EIS sensors help reduce electrode degradation and contribute to enhanced stability over time.

2. Literature Review

2-1. Glucose sensing in diabetic patients

Diabetes is a chronic condition resulting from abnormal insulin levels in the body [13, 14]. Insulin is essential for regulating glucose, as it allows cells to either use glucose for energy or store it for later. As a result, any disruption in insulin production can interfere with blood glucose balance, leading to high blood sugar levels (hyperglycemia) or low blood sugar levels (hypoglycemia). Diabetes is also linked to several serious health complications, such as coeliac disease, cystic disease, tuberculosis, and heart disease [15].

Given its significant impact on health, managing diabetes effectively has become a major focus. Research shows that maintaining strict blood sugar control can improve survival rates and help prevent complications associated with both type 1 and type 2 diabetes [13]. In recent decades, continuous blood glucose monitoring with sensor devices has proven essential for managing the condition.

Non-enzymatic sensors have been gaining popularity in various fields, particularly in biosensing and medical diagnostics, due to several key advantages over enzymatic sensors. The shift toward non-enzymatic sensors is driven by their improved stability, durability, and cost-effectiveness, among other factors[16]. Non-enzymatic sensors tend to have higher stability over time, making them more reliable for long-term use. These sensors are endowed with a broader operation conditions and lower cost, which makes them advantageous over enzymatic sensors. Particularly, non-enzymatic sensor is capable of continuous measurement of the bioanalytes, which offers a great potential for glucose monitoring. However, there are some inhibitory factors involved with their usage. While advancements have been made some nonenzymatic sensors lack

the high selectivity that enzymatic sensors provide, potentially leading to interference from other substances present in the sample [17].

Molecularly imprinted polymers are designed to have specific cavities that match the size, shape and chemical functionality of the target molecule. Their specificity allows for high sensitivity and selectivity in detecting target molecules (e.g. proteins, volatile organic compounds and metabolites). Therefore, they present a promising alternative in non-enzymatic detection due to their superiority in specificity and sensitivity compared to other non-enzymatic sensors. Waffo et al. also describes the artificial receptors as a method for the development of biomimetic sensors [18].

Molecularly imprinted polymers are generally more economical compared to enzyme-based sensors. Enzymes can be expensive and require complex storage conditions, while MIPs can be synthesized using simpler and cheaper materials. Furthermore, unlike some non-enzymatic sensors that require alkaline environments, MIP sensors can operate effectively in physiological conditions, making them suitable for applications in biological fluids like human serum (Figure 2-1).

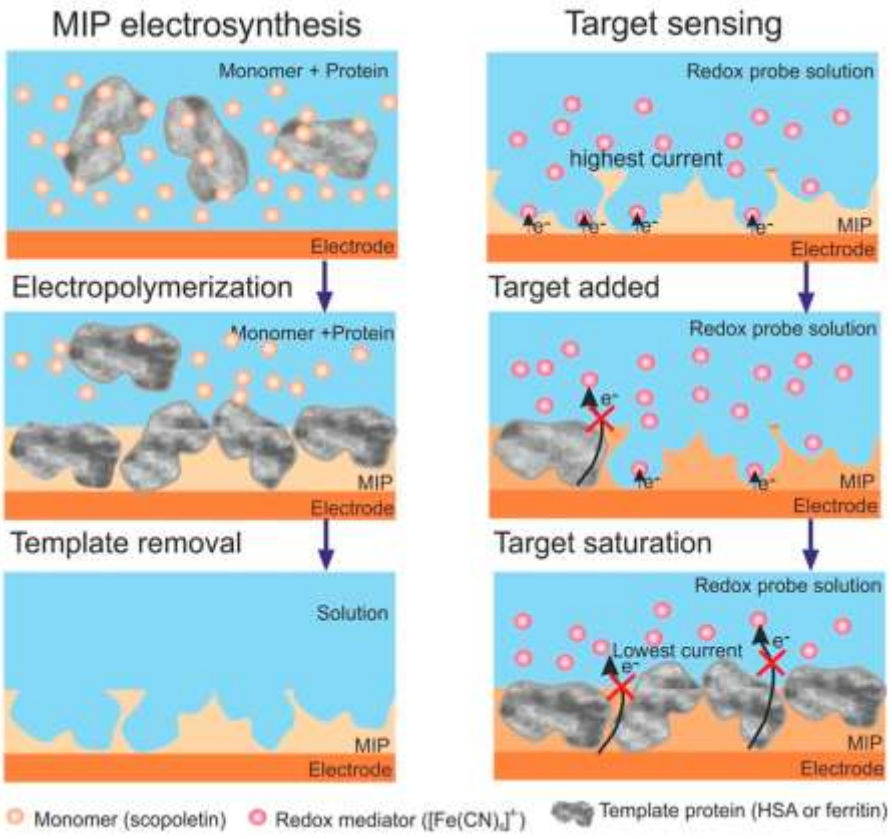

Figure 2-1 Schematic diagram of the surface-imprinted polyscopoletin nanofilm and its use for protein detection [19]

2-2. Different strategies for sensing Glucose

2.2.1- Glucose detection by enzymatic methods

The key feature of a blood glucose monitoring device is its detection technology, which measures glucose concentration. Since the development of the first enzyme electrode by Clark and Lyons in 1962, significant advancements have been made over the past 40 years to enhance its performance [20]. Most commercially available blood glucose monitors rely on an enzyme-based electrochemical method. Numerous studies have documented the ongoing improvements and advancements in blood glucose sensor technology.

Enzyme-based sensors, particularly those using glucose oxidase[1] and glucose dehydrogenase[2], are among the most widely employed technologies in glucose detection. While GOx is highly selective for glucose molecules, its performance is significantly affected by environmental factors. For instance, GOx loses activity in acidic or basic environments and becomes unstable at temperatures above 40°C [21]. Additionally, fluctuations in humidity can severely degrade the performance of GOx-based sensors, as the enzyme relies on a stable and hydrated environment for optimal activity. Other Enzymes such as glucose dehydrogenase (GDH) are catalyzing the oxidation of glucose to Gluconolactone, using a cofactor [22, 23]. This reaction generates electrons, which can be detected electrochemically. Although GDH exhibits higher activity compare to GO_x, its selectivity can be a concern since it can interact with multiple sugars present in a complex biological sample.

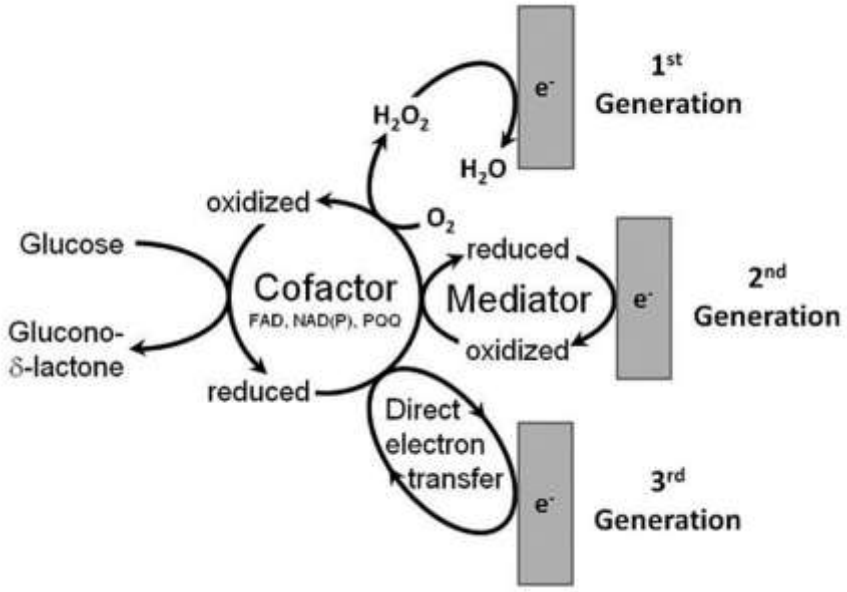

Figure 2-2 Schematic representation of the principles of first-, second-, and third-generation glucose sensors [22]

[1] GO_x
[2] GDH

2.2.2-Glucose detection by non-enzymatic methods

Most commercially available glucose sensors rely on enzyme-based detection mechanisms. To enhance their performance, various enzyme immobilization techniques have been developed, including direct adsorption, sol-gel encapsulation, cross-linking, and other advanced methods. These techniques, however, significantly influence the sensitivity and stability of the sensors, often leading to the deactivation of immobilized enzymes. Furthermore, enzyme-based sensors frequently encounter challenges related to complex fixation procedures and the requirement for engineered biological substances. Their functionality is particularly vulnerable to external factors such as temperature fluctuations, solvent exposure, and humidity variations during the manufacturing process, which can diminish their overall reliability and performance [24].

In contrast, non-enzymatic glucose sensors present several notable advantages. These sensors are structurally simpler, eliminating the need for complex enzyme immobilization and the associated challenges. Non-enzymatic sensors are also independent of oxygen availability, which is a limiting factor in the enzymatic approach. A key advantage lies in their enhanced robustness, as they are not as susceptible to environmental changes, including thermal and humidity variations, ensuring consistent performance under diverse conditions [24].

Moreover, the production of non-enzymatic sensors does not require the stringent sterilization protocols necessary for enzymatic electrode manufacturing, which simplifies the fabrication process and reduces operational costs. This lack of sterilization requirements not only streamlines manufacturing but also significantly lowers the unit price of glucose monitoring systems, making them more accessible. Additionally, non-enzymatic sensors often exhibit greater durability and longer operational lifespans compared to their enzymatic counterparts, further enhancing their

cost-effectiveness and appeal for widespread use in continuous glucose monitoring applications. These attributes make non-enzymatic sensors a promising alternative for glucose monitoring systems, offering improved reliability, cost efficiency, and adaptability to varying operational environments, which are critical for meeting the growing demand for advanced and accessible diabetes management technologies.

2.2.3-Background knowledge for non-enzymatic glucose electrochemical sensors

Mutarotation[3] is the process by which glucose interconverts between its cyclic forms, α-glucose and β-glucose, and its open-chain aldehyde form when dissolved in water. In aqueous solution, glucose predominantly exists in two cyclic structures distinguished by the orientation of the hydroxyl group attached to the anomeric carbon (C-1); in α-glucose, this hydroxyl group is positioned below the plane of the ring, while in β-glucose, it is above [25]. The interconversion begins when either cyclic form opens to form the linear aldehyde structure, which can then reclose to yield either the α or β form. This process occurs relatively slowly, often taking several hours to reach equilibrium, and is facilitated by acids or bases. As the α and β forms interconvert, the optical rotation of the solution changes, a phenomenon known as mutarotation, which is characterized by a specific equilibrium ratio of approximately 36% α-glucose and 64% β-glucose [26]. This dynamic equilibrium is significant in biological systems, as the different forms of glucose can exhibit varying reactivities and interactions with enzymes, and it is also crucial in analytical chemistry for measuring sugar concentrations based on optical rotation (Figure 2-3) [27].

[3] MR

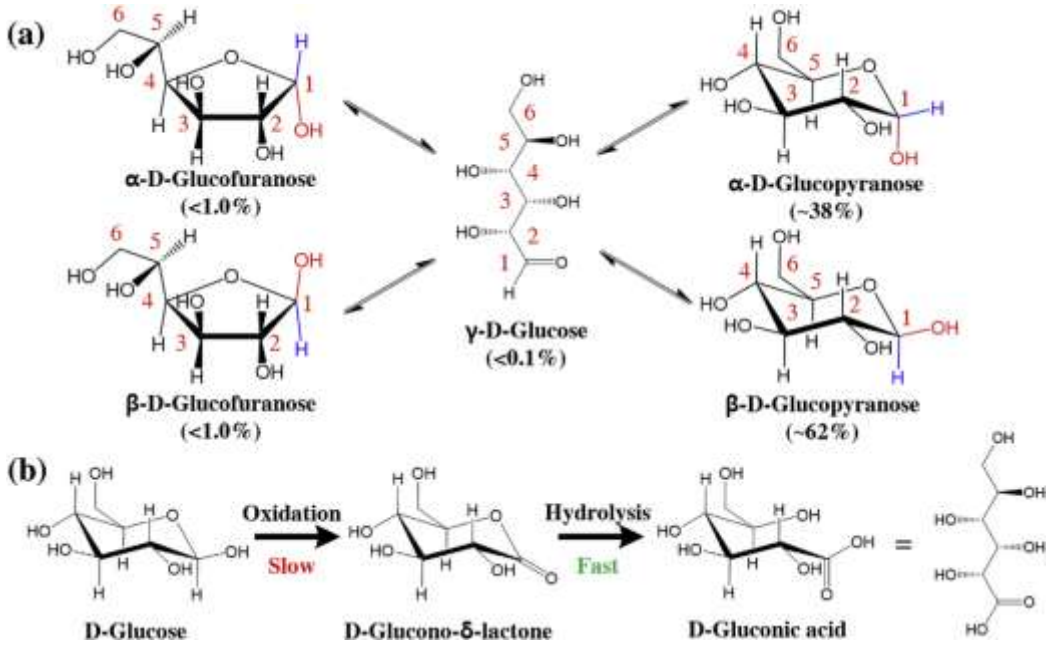

Figure 2-3 (a) Molecular structures of various D-glucose isomers (b) Overall process of glucose oxidation. The reaction proceeds from D-glucose into D-glucono-d-lactone via slow hydrogen abstraction and oxidation, followed by fast hydrolysis into D-gluconic acid [27]

2.2.3.1- Brief explanation of electrochemical glucose biosensor

The initial design of their glucose enzyme electrode involved immobilizing a thin layer of glucose oxidase (GOx) on top of an oxygen electrode, secured with a semipermeable dialysis membrane. The glucose concentration was determined by tracking the decrease in oxygen levels as it was consumed during the enzyme-catalyzed reaction.

$$Glucose + O_2 \xrightarrow{Glucose\ Oxidase} Gluconic\ acid + H_2O_2 \quad (1)$$

A negative potential was applied to the platinum cathode for a reductive detection of the oxygen consumption. The origins of the biosensor field can be traced back to the development of the first glucose enzyme electrode. Clark's pioneering patent laid the foundation by describing how enzymes could be used to convert electro-inactive substances into electroactive products, making them detectable via electrochemical methods [28]. To reduce interference, he proposed a dual-

electrode system—only one of which was enzyme-coated—allowing the differential current to be measured for more accurate results. This innovation led to the creation of the first commercial glucose analyzer, developed by Yellow Springs Instrument (YSI) Company in 1975. Known as the YSI Model 23, it enabled direct glucose measurement from small whole blood samples (25 µL). Building on Clark's concept, Updike and Hicks refined the system by using two oxygen-sensitive electrodes to compensate for background oxygen fluctuations [29]. Later, in 1973, Guilbault and Lubrano advanced the technology further by introducing an enzyme electrode that measured blood glucose through the anodic detection of hydrogen peroxide generated during the enzymatic reaction [30].

$$O_2 + 4H^+ + 4e^- \rightarrow 2H_2O \quad (2)$$

The developed biosensor demonstrated reliable accuracy and precision when used with 100 µL blood samples. Since then, a diverse array of amperometric enzyme electrodes has been reported, varying in electrode architecture, materials used, enzyme immobilization techniques, and membrane compositions.

Also, the electro-oxidation of glucose was investigated on many electrodes including: carbon, copper, platinum and gold electrodes utilizing cyclic voltammetry in basic environment [31]. In case for platinum, the electrolysis of D-glucose was carried out at two oxidation potentials: 0.70 and 1.1 V_{RHE}. For both of the oxidation potential, gluconic acid is the main product of the electrochemical reaction based on the previous literature. The electrolysis of D-glucose on gold electrode was also studied on gold electrode, which resulted in two oxidation potentials of 0.55 V and 1.34 V_{RHE}; in the lower oxidation potential, 0.55 V_{RHE} the glucose exclusively converts to gluconic acid, while at higher potential, 1.34 V_{RHE}, part of the glucose further converts to glucaric

acid through oxidation of both, the aldehyde and the hydroxymethyl group. Other studies that involve electro-oxidation of glucose on a carbon electrode reported an amperometric detection of glucose at 0.9 V versus Ag/AgCl [32].

2.2.4- Direct glucose oxidation via metallic redox centers

Electrocatalytic processes work through a mechanism called adsorption, where reactant molecules attach themselves to the active sites of an electrode. Several factors influence this process, such as the electronic properties of the redox center, the presence of unfilled d-orbitals in transition metals, or defects in non-metallic materials [33, 34]. Once the reactant is adsorbed, chemical bonds break, and intermediates are formed. As the oxidation state of the redox center changes, the bond between the product and the electrode weakens, allowing the product to detach from the surface. This cycle of adsorption and desorption is commonly referred to as the chemisorption model [35].

In the case of glucose oxidation based on the chemisorption model, the interaction between the glucose molecule's C-1 atom and its hydrogen with the electrode surface intensifies as the molecule nears the electrode. This leads to dehydrogenation at C-1 and adsorption onto the electrode. The adsorbed glucose undergoes electro-oxidation to form glucono-d-lactone, which is further oxidized to gluconic acid through different reaction pathways depending on the pH of the environment [36]. The reactive hydroxide species (OH_{ads}) that form on the electrode surface during electrocatalysis play a crucial role in redox reactions involving small organic molecules. These surface-bound hydroxide radicals actively oxidize the reactants [36, 37]. To better understand this process, Burke and his team introduced the incipient hydrous oxide/adatom mediator (IHOAM) model [37]. This model provides a complementary explanation for the complex nature of

electrocatalysis, working alongside the chemisorption-based model to describe these reactions in greater detail [38].

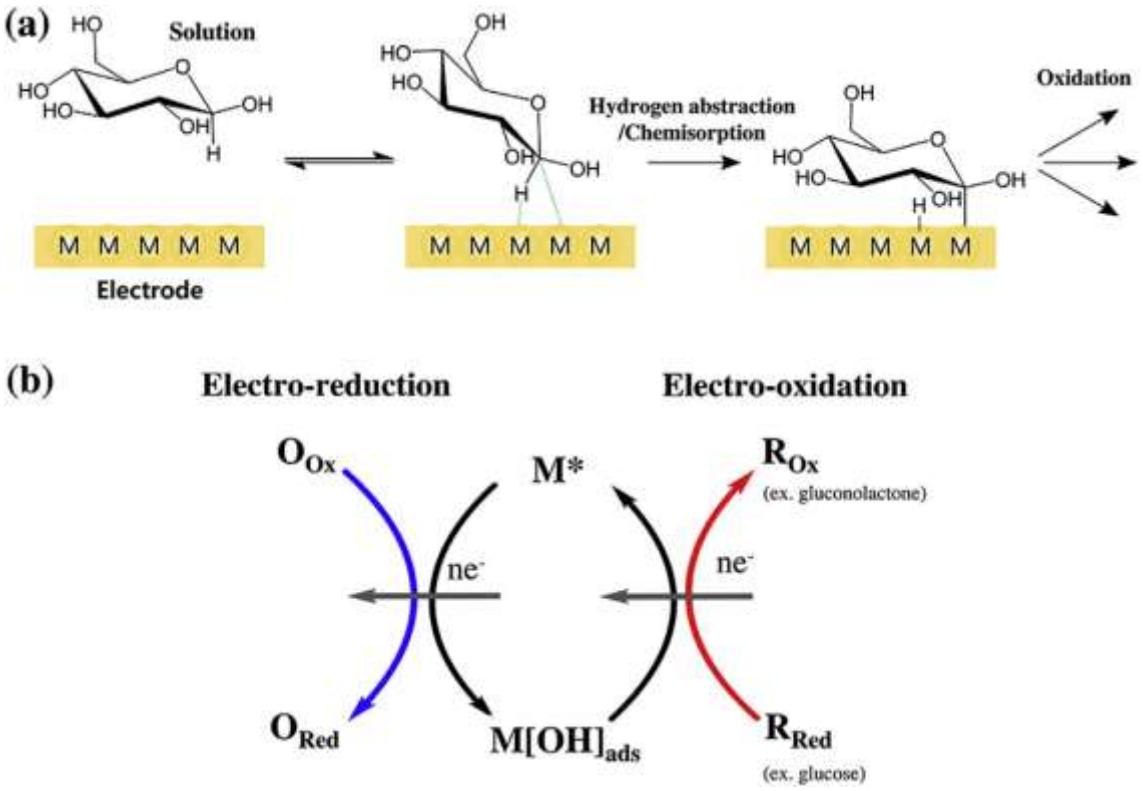

Figure 2-4 (a) The chemisorption mechanism of glucose oxidation. (b) Incipient hydrous oxide/adatom mediator model[38]

The chemisorption and IHOAM models primarily focus on noble metal electrodes, such as platinum (Pt) and gold (Au), making them less applicable to transition metals or metal oxide-based electrodes [39]. For these materials, the redox behavior of the transition metal centers provides a better explanation for glucose oxidation, as seen with metals like nickel (Ni), copper (Cu), and cobalt (Co). Under anodic bias, a metal oxide layer with a lower oxidation state (lower oxide) is transformed into a higher oxidation state (higher oxide) [39]. This higher oxide possesses strong oxidative properties, enabling it to generate surface bound OH_{ads} radicals capable of oxidizing

nearby organic reactants. The oxidative adsorbed hydroxide radical expressed as MOH_{ads} is formed by the chemisorption of hydroxide anions to the reductive metal adsorption site (expressed as M as shown in the following equation) and is believed to be the catalytic component of electrocatalysts for glucose.

$$H2O \rightarrow H^+ + OH^- \quad (3)$$

$$M + OH^- \rightarrow MOH_{ads} \quad (4)$$

The initial step in glucose oxidation involves the removal of the hydrogen atom from the C-1 position. This is followed by further oxidation of the reaction intermediates, resulting in the formation of glucono-d-lactone [40]. Although the exact mechanisms remain unclear, these processes likely involve interactions with surface hydroxyl radicals, hydroxide ions, or solvent molecules present in the reaction solution [41].

2.2.5- Nonfaradaic detection via association with glucose

Glucose sensor technologies often use biomaterials such as glucose-oxidizing enzymes (GOx and GDH), glucose-binding lectins (e.g., concanavalin A), and glucose-specific dextrans, which rely on selective interactions between glucose molecules and their active sites [42-44]. However, since the early 2000s, researchers have explored electrochemical methods using synthetic materials instead of biomolecules. These efforts can be grouped into two main categories: materials incorporating boronic acid functional groups and molecularly imprinted polymers with functionalities like amines, hydroxyl, and carboxylic groups. However, since the early 2000s, researchers have explored electrochemical methods using synthetic materials instead of biomolecules. These efforts can be grouped into two main categories: materials incorporating

boronic acid functional groups and molecularly imprinted polymers with functionalities like amines, hydroxyl, and carboxylic groups.

Boronic acid features a central boron atom bonded to two hydroxyl groups and an alkyl or aryl group, arranged in a trigonal planar structure due to sp^2 hybridization. The boron's vacant p-orbital is reactive to incoming nucleophiles. Unlike carboxylic acid, boronic acid's hydroxyl groups are not easily deprotonated. Instead, the boron atom behaves as a Lewis acid, forming Lewis acid-base pairs with nucleophiles, releasing H^+ in the process. Boronic acid can reversibly form diesters with 1,2-diols and 1,3-diols, demonstrating a strong affinity for polyols like carbohydrates [45, 46]. This makes boronic acid a promising functional group for saccharide detection. However, selectively detecting glucose remains challenging due to boronic acid's inherent affinity for all types of diols, not just glucose.

Boronic acid-based functionalities generally exhibit similar reactivity toward most saccharides. However, the formation of boronic diesters doesn’t produce electrochemical signals, particularly faradaic signals [43]. Because of this limitation, boronic acid is often used in sensing techniques like colorimetry, fluorescence, and absorbance rather than electrochemical methods.

To enable the use of boronic diester formation in electrochemical glucose sensing, three strategies have been developed. The first approach involves potentiometry, which monitors the potential changes of electrodes functionalized with boronic acid. These electrodes, often made from conducting polymers or gold nanoparticles, detect glucose by measuring the equilibrium potential shifts caused by glucose binding. This method works without requiring redox reactions, allowing for electrochemical glucose detection [47].

The second strategy introduces a redox marker that is repelled when the gluco-boronate ester forms on the electrode. The negatively charged redox marker, such as $Fe(CN)_6^{3-/4-}$ [48], is

electrostatically pushed away from the negatively charged boronate ester on the electrode surface. As glucose concentration increases, the redox current decreases, surface resistance changes, or differences between anodic and cathodic peaks become more noticeable [49].

The third approach directly measures redox currents using electrodes functionalized with boronic acids coupled to conducting polymers or redox markers [50, 51]. Techniques like differential pulse voltammetry (DPV) are particularly effective for this method. When boronate esters form, they induce structural changes in the functionalized electrodes, leading to altered redox currents or shifts in redox peaks. DPV is preferred because it minimizes the risk of over-oxidizing sensitive materials like conducting polymers.

MIPs are specialized polymer structures designed with functional groups that selectively bind to a target analyte. These polymers have been explored for detecting a wide variety of biomolecules, such as proteins, neurotransmitters, and DNA, as well as organic compounds like toxins, drugs, and pollutants [50, 52]. The process involves mixing functionalized monomers containing groups like amines, carboxylic acids, hydroxyls, and aryl groups with the target analyte. These monomers are then polymerized, or "imprinted," while bound to the target. This creates a mold capable of recognizing and binding to even highly complex structures with specificity.

MIPs have gained significant attention for their versatility and selectivity, making them appealing for use in optical sensors (like fluorescence and absorbance-based systems) and electrochemical sensors. However, research on using MIPs for detecting small, simple molecules like glucose is limited. This is primarily due to challenges in glucose detection, such as slow sensor response times and the need to carefully maintain equilibrium conditions like pH, temperature, and ion concentrations.

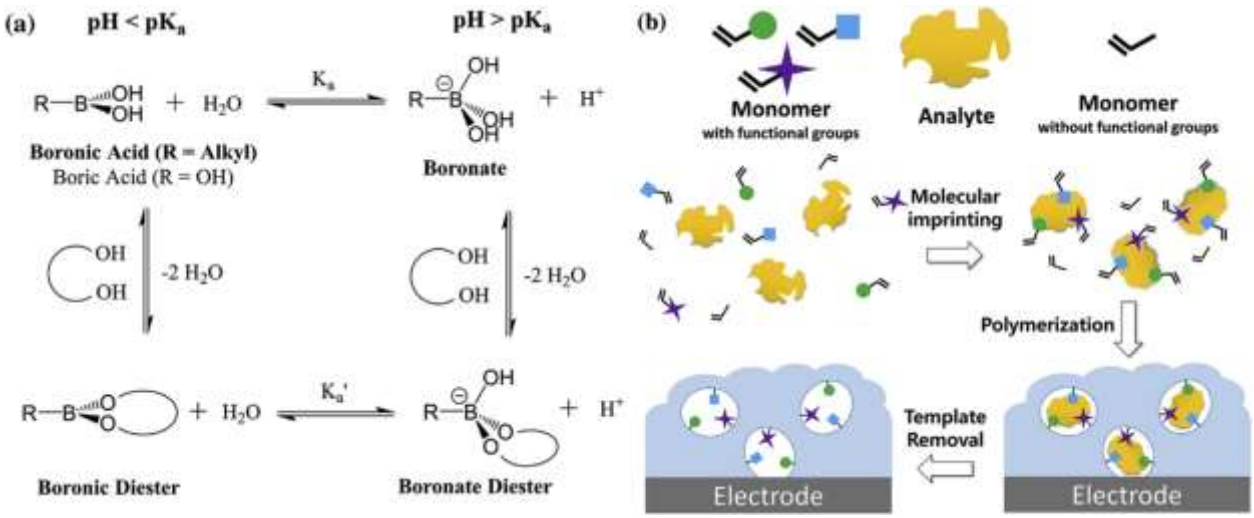

Figure 2-5 (a) The possible equilibria of bor(on)ic acid and diols in aqueous solution. The boronic and related compounds easily form diesters 1,2- and 1,3-diols.[53] (b) Schematic representation of molecular imprinting by non-covalent interactions between the analyte and functional monomers. The molecularly-imprinted polymer selectively rebinds to molecules matching the imprinted binding sites, analogous to the binding sites of biomolecules such as enzymes and receptors [52]

In this research, a strategy utilizing impedance spectroscopy to detect glucose at varying concentrations has been implemented with the aid of the MIP. Molecularly imprinted polymers provide a highly selective and sensitive approach to sensor design due to their ability to form specific recognition sites that mimic the target molecule. The use of redox markers, combined with boronic acid-based sensing, further enhances the electrochemical detection of glucose. Boronic acid-based sensors are particularly advantageous as they can reversibly bind to diol-containing compounds like glucose, enabling robust and reliable glucose detection. The synergy between MIP sensors and boronic acid functionality significantly improves the selectivity, stability, and sensitivity of the sensor, offering a promising avenue for advanced glucose monitoring applications.

Below, we explore different strategies to capture glucose using the imprinting technique, recognizing the insurmountable ability of MIPs for electrochemical sensors targeting diabetic

biomarkers. These strategies underscore the potential of MIPs to revolutionize the detection of glucose and other critical biomarkers in diabetes management.

2-2-6. Molecularly imprinted polymers-based electrochemical biosensors

2.2.6.1. Electrochemical synthesis of MIPs

Eelctropolymerization introduces several advantages for realizing MIPs for sensing purposes and aiming at a reliable interface between the recognition element and the sensor transducer. It is worth mentioning that the lack of initiators in this method introduces major advantage over thermally, chemically, or UV light-initiated polymerization, in which he structures of the templates are subjected to change and deactivating the protein/enzyme. The fabrication of MIPs can be controlled with the different electrochemical parameters (transferred charge, current or Voltage chages) to optimize the thickness of the layer that is deposited onto the surface of the electrode. Also, Electropolymerization enables the synthesis of MIPs under gentle conditions, such as in aqueous environments and at room temperature, making it particularly suitable for imprinting biological molecules like proteins. Numerous research has been conducted to figure out the charactersitics of imprinting techniques and their method of action; here we summarize the notable fabricate MIPs for detecting biological molecules.

Syritski's group developed an electrochemical surface imprinting strategy successfully applied to imprint immunoglobulin G, cerebral dopamine, brain-derived neurotrophic factors (CDNF and BDNF), and SARS-CoV-2 proteins. The method involves (A) covalent immobilization of the target protein via a cleavable linker on a conductive surface, (B) controlled electropolymerization to avoid protein entrapment, (C) linker cleavage for protein removal, and (D) formation of MIPs

with protein-specific binding sites on the polymer surface. This approach enables highly selective and sensitive protein detection (Figure 2-6).

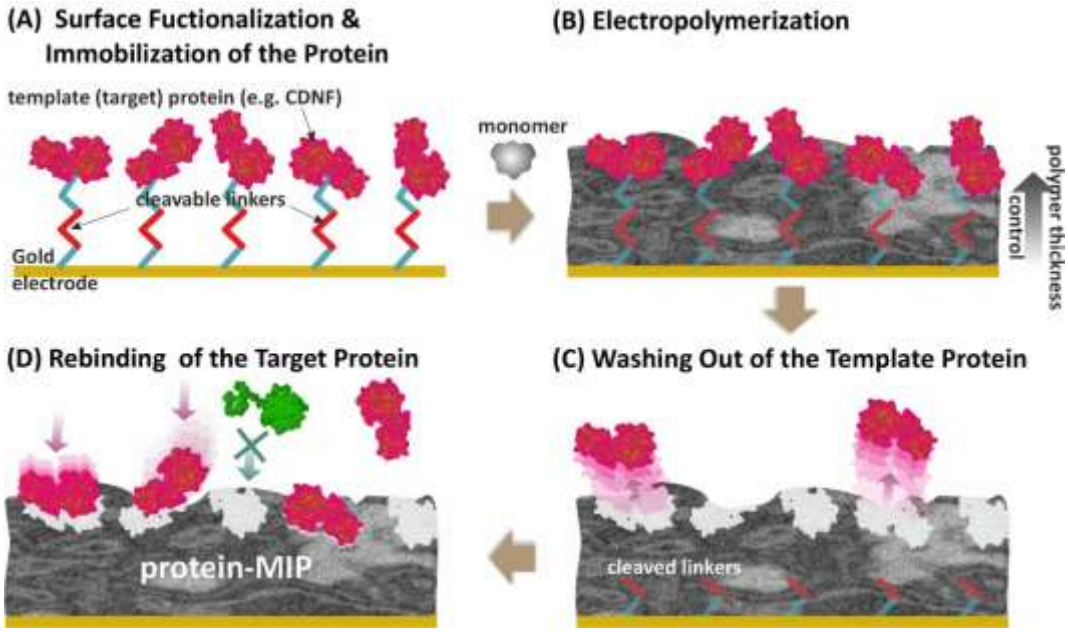

Figure 2-6 The surface imprinting strategy for the synthesis of a protein-MIP layer on a conducting surface using the electropolymerization approach. The strategy consists of (A) covalent immobilization of a target protein via a cleavable linker to a conducting surface; (B) electropolymerization of a monomer with careful control of the thickness of the growing polymer to exclude protein entrapment; (C) cleavage of the linker to facilitate protein removal; and (D) formation of MIP with protein-selective binding sites located on the polymer surface [48].

Researchers in Poland also developed a surface imprinting technique combining colloidal crystal templating with electropolymerization to create an inverse opal structure with molecular imprints on the surface. This method began with the preparation of a hierarchical colloidal crystal template using SiO_2 nanoparticles (NPs), typically assembled via the Langmuir–Blodgett technique (Figure 2-7A). Template protein molecules, such as human chorionic gonadotropin (hCG), were then immobilized onto the surface of these NPs (Figure 2-7B) and functionalized with monomers like bithiophene (Figure 2-7C). Electrodeposition of a poly(2,3′-bithiophene) film within the hierarchical template followed (Figure 2-7D). Finally, the removal of NPs and proteins yielded a polymeric inverse opal material with molecular cavities exclusively on the inner pore

walls (Figure 2E). This innovative approach produced a highly porous hierarchical MIP nanostructure with exceptional sensitivity for target protein detection.

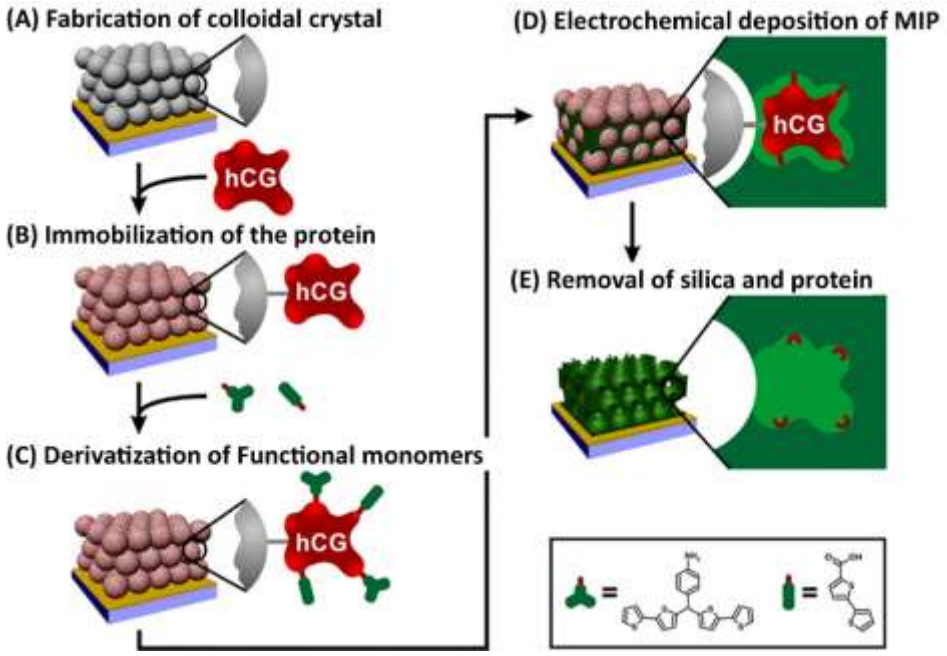

Figure 2-7 A surface imprinting approach combines colloidal crystal templating with electropolymerization to fabricate an inverse opal structure with molecular imprints of a protein (e.g., hCG) on the surface. The approach includes the following steps: (A) fabrication of a colloidal crystal template of SiO2 NPs; (B) immobilization of target protein (hCG) on the surface of NPs; (C) derivatization of protein with functional monomers (bithiophene); (D) electrodeposition of poly(2,3′-bithophene) film; (E) removal of NPs and the protein from the polymer, resulting in a polymeric inverse opal material with molecular cavities on the inner side of the pore wall [54]

2.2.6.2- Electrosynthesized MIP-based sensors for detection of saccharides

As discussed earlier, most MIP-based electrochemical sensors don't rely on directly oxidizing or reducing analytes to generate an electrochemical signal. Instead, an indirect approach using a redox probe is often preferred because it provides more practical and reliable results. In this method, the electrochemical behavior of a redox probe is monitored in a solution with either a template-extracted or template-bound MIP film. For instance, when hexacyanoferrate was used as a redox probe, the cyclic voltammograms showed clear differences depending on whether the template molecule was present or absent on the MIP-modified electrode (Figure 2-8). This process,

known as the “gate effect,” was first introduced by Yoshimi et al. in their work on an acrylic MIP-based chemosensor.

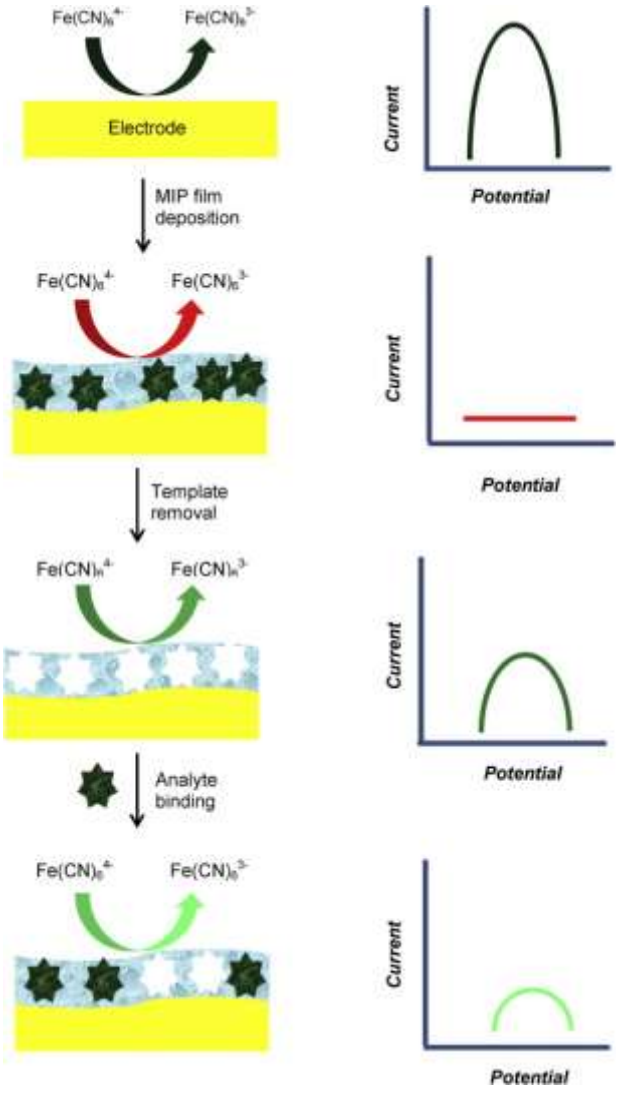

Figure 2-8 Examples of using “gating effect” for indirect electrochemical detection of the analyte at the MIP-based electrode and the corresponding current potential signals [55]

Initially, scientists assumed the binding of target analyte molecules by molecular imprints caused the swelling of MIP film, which leads to pore expansion in the film, resulting in the increase faradic current corresponding to the oxidation of redox probe at the electrode-MIP film interface. However, it was later found out that analyte binding can also hinder faradic probe current. The

topography and the thickness of the MIP-bound layer has a striking effect on the suppressed or enhanced diffusion.

In a novel method of fabricating smart MIPs, saccharide-templated MIPs derived from 3-aminophenylboronic acid (3-APBA) were developed for the detection of fructose [56]. This research proposed the formation of a (D-fructose)-APBA complex within a polyaniline (PANI) matrix, which maintained high conductivity at elevated pH levels. This allowed for effective complexation between saccharides and aromatic boronic acids. Later, D-fructose was removed from the polymeric network by soaking the carbon electrode overnight in phosphate-buffered saline (PBS) at neutral pH conditions (pH 7.4). Further research revealed that introducing fluorine (F_2) groups enhanced the electropolymerization of the saccharide complex with 3-APBA, simultaneously leading to the formation of a self-doped polymer.

In another study, Zhang et al. explored the selective recognition of epinephrine (EP) using poly-APBA[57]. The EP-imprinted MIP film was prepared through potentiodynamic electropolymerization under slightly alkaline conditions (pH 8). The entrapped EP molecules were removed using both chemical and electrochemical methods. The researchers explained that the enhanced electrochemical response was attributed to the abundance of imprinted cavities containing boric acid groups, which selectively adsorbed epinephrine molecules. Additionally, the synergistic effect between multi-walled carbon nanotubes (MWCNTs) and the PAPBA layer contributed to the improved performance (Figure 2-9).

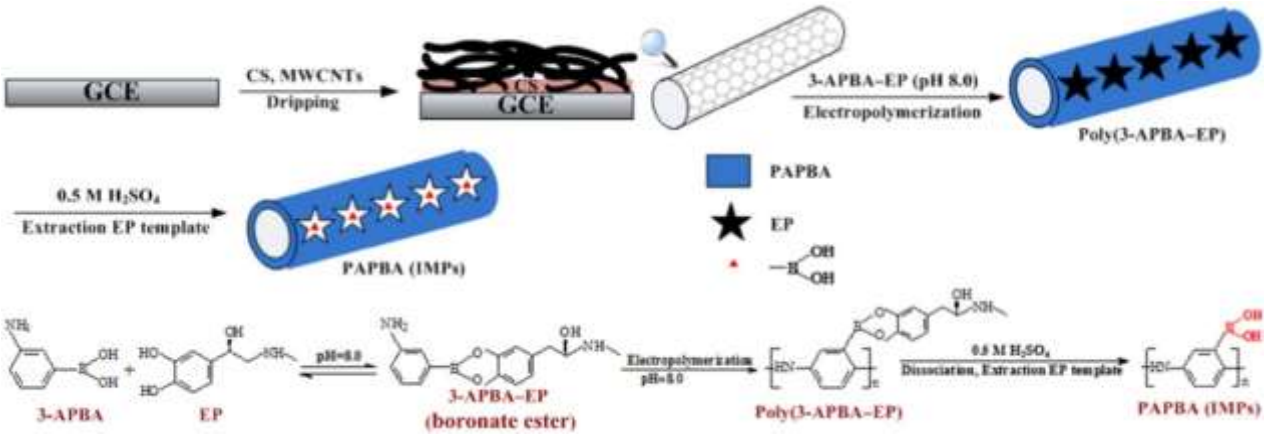

Figure 2-9 Graphical depiction of the constructed EP-imprinted biosensor preparation[57]

There are also some of the glucose MIP-based sensors, which use amperometry or other electroanalytic techniques in order to study surface changes upon rebinding of an analyte or the presence of the analyte in the solution. For instance, Cho et. al. reported the fabrication of a selective MIP glucose sensor based on the direct oxidation of the glucose on a metallic catalyst with MIP. This study revealed a heightened performance in artificial as well as whole blood samples using chronoamperometry technique.

In this research, we further explored the interesting capabilities of electro-synthesized MIPs in leaving a biomolecule-shaped behind, which can be potentially executed to detect the captured glucose. In this research, several characteristics of the synthesized MIP has been reviewed. First, the ability of boronic groups to form a complex with the glucose has been investigated. Secondly, the characterization of each deposition steps has been explored to ensure the effective creation of the desired sensor. Thirdly, the MIP and NIP comparison has been done to make sure the effective fabrication of sensor. Next, the optimization of the effective parameters in synthesizing a operable sensor have been closely observed. Lastly the performance of the MIP sensor has been analyzed

and a conclusion were drawn based on the sensitivity, linear range, diffusion rate and stability assessment.

2-4. Motivation and Objective

My research is focused on developing a non-enzymatic sensor aimed at enhancing the performance of glucose detection systems. This study investigates the superior stability and sensing efficiency of MIP based sensors while addressing the cost-related inefficiencies associated with expensive, single-use enzymatic kits. By leveraging the robustness and reusability of MIP sensors, this work has significant implications for advancing portable and real-time glucose monitoring technologies. Given the financial burden that single-use diagnostic kits impose on patients with diabetes, the proposed non-enzymatic sensors offer a cost-effective alternative with improved durability and consistent sensing performance. Furthermore, the exceptional stability of MIP-based sensors makes them ideal candidates for integration into wearable devices, facilitating continuous and convenient glucose monitoring for better diabetes management.

2-5. Thesis Outline

The synthesis of APBA-functionalized MWCNTs and imprinting layers, characterizations of layers, sensor preparations and performance are all presented in Chapter 3. Next, the materials and sensing characterization results are depicted in Chapter 4. At the end, a brief review of the achievements, contributions and future works are presented in Chapter 5.

3. Materials & Methodology

3-1. Materials and Methods

In this section, a list of the main materials used in this study and where they were obtained from is presented. These materials were crucial in conducting the experiments and synthesis conducted throughout the study, and their selection was based on their properties and suitability for the intended purposes.

All chemical reactants and reagents used in this research were of analytical grade and were used as received without further purification. Tris(hydroxymethyl) aminomethane,acs reagent, ≥99.8%, N-(3-Dimethylaminopropyl)-N'-ethylcarbodiimide hydrochloride (EDC), N-Hydroxysuccinimide (NHS), Solid, 98%, Poly bottle, ReagentPlus® Sodium phosphate monobasic, Powder, ≥99.0%, Poly bottle, Sodium phosphate dibasic ReagentPlus®, ≥99.0%, crystalline Potassium hexacyanoferrate ($K3[Fe(CN)6]$, ≥99.0 %) and Potassium hexacyanoferrate (II) trihydrate ($K4[Fe(CN)6]\cdot 3H2O$, ≥98.0 %) were acquired from Sigma Alderich (St. Louis, MO, USA). The carbon nanotubes, muti-walled (D*L 50-90 nm), >97.0% Pyrrol, 3-Aminophenylboronic acid (3-APBA) were prepared from Sigma Aldrich. The screen-printed carbon electrode (SPCE) was purchased from Zensor, consisting of a carbon working electrode (exposed area of 0.071 cm2), a carbon counter electrode, and an Ag pseudo reference electrode. Ultrapure water (18.2 MΩ·cm) was used for all washing processes. Electrochemical electro- polymerization and measurements employed the Autolab potentiostat (Ultrecht, Netherlands, Metroohm), which were controlled by the NOVA software. Sulfuric acid (>98%) and hydrogen peroxide (35 wt. %) were used as functionalizing liquids supplied from Sigma-Aldrich. All experiments conducted at room temperature (25 ± 2 ◦C).

3-2. Synthesis of MWCNT-COOH

3-2-1. Pirranha-treated MWCNTs

In a typical procedure, 300 mg of MWCNTs (Nanotech Port, China) were measured out and placed in a 100 mL round-bottom flask. Next, 75 mL of concentrated sulfuric acid (H_2SO_4) was added. To ensure the mixture was evenly dispersed, it was sonicated for about 5 minutes. After that, 25 mL of a 30% H_2O_2 (Univar, Ajax APS) was slowly added to the mixture to prevent it from overheating. The resulting mixture was then stirred continuously at 500 rpm using a magnetic stirrer and left to react under reflux conditions for 5 hours at room temperature. Once the reaction was complete, 100 mL of Milli-Q water was added to stop the process. The mixture was then washed several times with Milli-Q water until the pH reached a neutral level.

Finally, the piranha-treated MWCNTs (p-MWCNTs) were separated by centrifugation and dried in an oven set at 40°C.

3.2.2- Hydrothermal Treatment

Hydrothermal treatments were carried out using a 50 mL Teflon-lined stainless-steel autoclave. To start, 50 mg of multi-walled carbon nanotubes (MWCNTs) were mixed with 35 mL of Milli-Q water. The mixture was sonicated for 5 minutes to ensure it was well-dispersed and then transferred into the autoclave.

The autoclave was placed in an oven and left there for 18 hours, with the treatment temperature set as needed. Once the process was complete, the treated MWCNTs were recovered by centrifugation. No additional purification steps were performed afterwards (Figure 3-1)

Figure 3-1 The protocol for Synthesizing surface-oxidized MWCNTs

This method ascertains the formation of ketonic and carboxylic groups, enabling surface oxidation groups to functionalize the surface of MWCNTs with groups such as hydroxyl, epoxy and carboxyl. This reaction results in better dispersion of MWCNT in water and a further modification with other catalysts.

3-2-3. Preparation of APBA-MWCNT Nanocomposites

The oxidized MWCNTs were dispersed in ultrapure water to achieve a concentration of 1 mg/mL. While stirring rapidly, EDC (0.05 g) was added quickly, and the mixture was continuously stirred at room temperature for 1 hour. Next, NHS (0.1 g) was added to the suspension. Subsequently, APBA (0.05 g) was added, and the solution was stirred overnight at room temperature. The APBA-functionalized MWCNTs were then rinsed with ultrapure water and re

dispersed in ultrapure water at a concentration of 1 mg/mL as illustrated in Figure 3-2. At last, a grey solution of APBA-MWCNT is resulted.

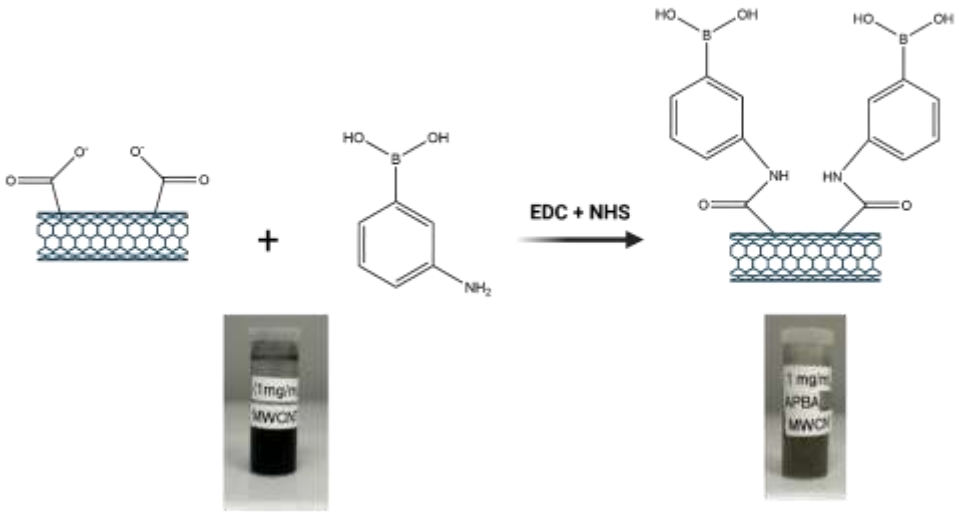

Figure 3-2 The Mechanism for synthesis of MWCNT-APBAs

3-3-Electrochemical technique for developing biomimetic sensors

Recently, study of electrochemical biosensors has been a highly-noticed area in the field of sensors. Firstly, most of the electrochemical sensors are fairly cheap to develop compared to other sensors in the market. Secondly, the working area of the electrodes are easily modifiable which offers a reliable way to study selectivity and sensitivity of the sensors. Lastly, electrochemical devices can produce higher signal to noise ratio (S/N) which, in turn, favors their use against more complicated methods of detection [58].

Our electrochemical setup is displayed at theFigure 3-3, which shows the simplicity of acquiring sensor information, apart from the Autolab potentiostat, which is also available in much

smaller shape. As soon as the electrical signals gathered from the SPCE sensor, the potentiostat sends these data to the device and the response is sent back to a computer for analysis

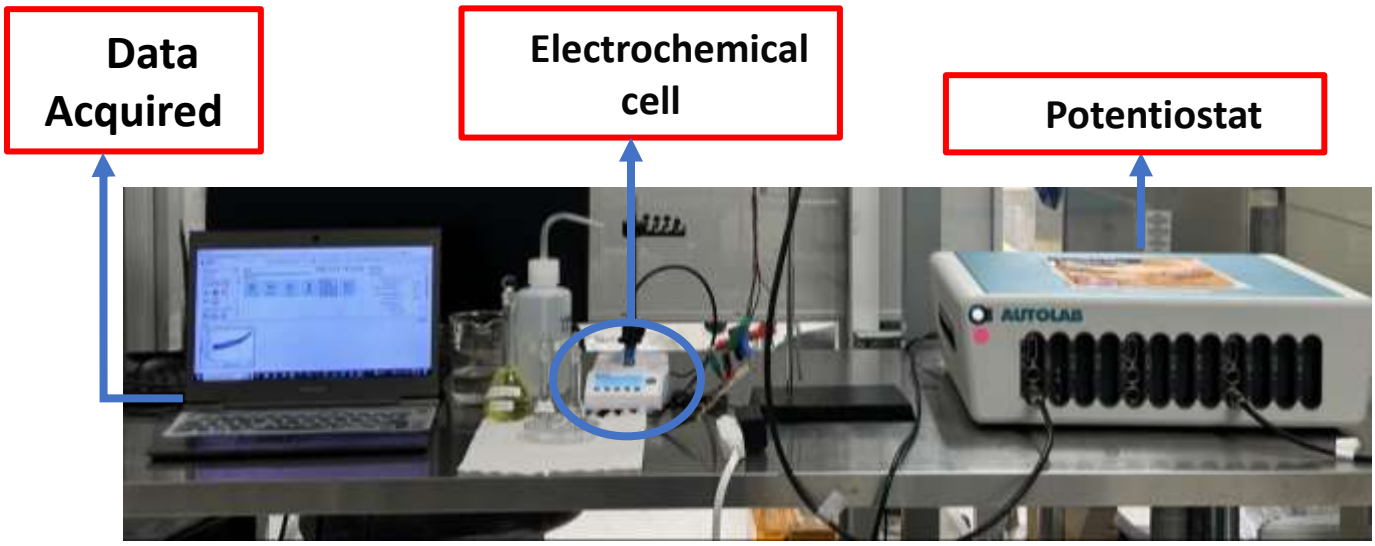

Figure 3-3 The electrochemical setup for sensing glucose

3-3-1. Electrochemical Cell

An electrochemical cell is defined an instrument that can transduce a chemical reaction to an electric signal. In addition, electrochemical biosensors always contain an analyze to measure current, voltage and impedance in the cell. As it is apparent in the Figure3-4, an electrochemical biosensor contains a working electrode (WE), counter electrode (CE), and Reference Electrodes (RE).

In our Screen-printed carbon electrode[4], working and counter electrodes are made of carbon. The reference electrode, on the other hand, is made of Ag pseudo, which can also provide a constant potential (Figure 3-5). This type of electrode is commonly utilized in research due to its ease of modification, stable electrical properties, and affordability. For electrochemical

[4] SPCE

measurements, 50 µL of solution is applied to the surface of the device, ensuring complete coverage of the WE, CE, and RE.

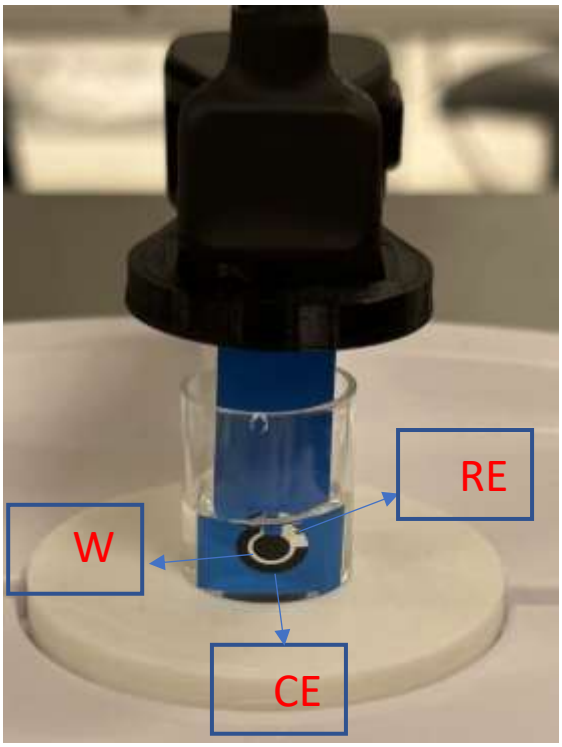

Figure 3-4 Our three-electrode system device

3-3-2. Electrochemical Measurements

In this work, DPV, square-wave voltammetry and EIS have been utilized to study the electrochemical properties of the MIP sensors and detect glucose's concentration in the solution.

Once the desired potential is applied o the WE of the electrochemical cell, the RE is used to control the potential of the working electrode without any current flow.

3-3-2-1. Cyclic Voltammetry

This technique is the most often technique used in electrochemical characterization and provides initial information about the heterogenous redox reactions . In this technique, the potentials sweep linearly from an initial value E_i, to a final value E_f an then back to E_i.

As the typical reversible redox couple of $Fe(CN)_6^{3-}/Fe(CN)_6^{4-}$ suggests for a platinum electrode, the main parameters of a cyclic voltammograms are: anodic peak current (i_{pa}), cathodic peak current (i_{pc}), anodic peak potential (E_{pa}) and cathodic peak potential (E_{pc}).

$$Fe(CN)_6^{3-} \underset{-e}{\overset{+e}{\rightleftharpoons}} Fe(CN)_6^{4-} \qquad 3\text{-}1$$

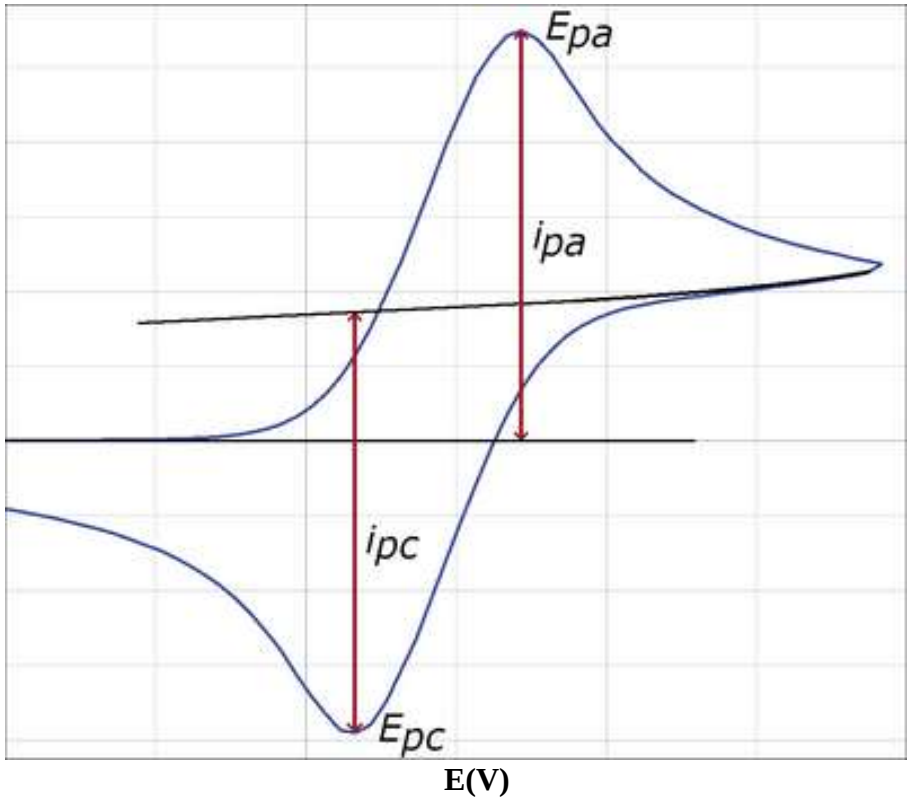

Figure 3-5 Typical cyclic voltammogram of 0.1 mM K3Fe (CN)6 in 1.0 M NaN03 on bare platinum

A redox pair where both species are stable and can rapidly transfer electrons to and from the working electrode is referred to as an electrochemically reversible couple. For such a reversible system, the formal reduction potential (E°) is the midpoint between Epa and Epc:

$$E^0 = \frac{Ep_a + Ep_c}{2} \qquad 3\text{-}2$$

For the forward sweep of the first cycle, the peak current can be determined by Randle-Sevick equation:

$$i_p = 2.69 \times 10^5 n^{3/2} A D^{1/2} C v^{1/2} \qquad 3\text{-}3$$

where ip is the peak current (amperes); n is the electron stoichiometry (eq/mol); A is the electrode area (cm^2); C is the concentration (mol/cm); v is the scan rate (volts/sec). According to this equation, ip is proportional to $v^{1/2}$ and the concentration of analyte species.

Cyclic voltammetry is a valuable tool for polymer characterization, as it helps identify key electrochemical properties. It can determine the potential at which the polymer undergoes reversible oxidation or reduction in a specific electrolyte, the potential where irreversible overoxidation occurs, and any changes in the polymer's electrochemical behavior caused by interactions with analytes in solution.

Additionally, cyclic voltammetry is useful for studying the electrochemistry of the monomer used for electro polymerization. By analyzing the voltammogram, the oxidation potential of the monomer can be identified, which helps define the potential limits required for the potentiation polymerization process.

In this work, cyclic voltammetry was done either to deposit the final layer of polymer to create the imprinting effect or to characterize the deposited layers in the redox probe. Regarding the characterization of each layers, voltage swept from -0.2v to 0.7v in 100mv/s in 2.5mM $Fe(CN)_6$.

Furthermore, the elecropolymerization of Pyrrole (40mM)/APBA (15Mm) layer was performed in PBS (pH=8) under the following optimized conditions: 8 cycles, 40mv/s, -0.4_0.9 voltage range.

3-3-2-2. Chronoamperometry

In chronoamperometry, the potential is quickly changed from an initial value (E_i) to a final value (E_f) in an instantaneous step. The resulting current is then measured over time. When the potential is stepped from E_i to E_f, a sharp increase in current occurs initially, followed by a gradual decrease. This decline is caused by the depletion of electroactive species at the electrode surface due to electrolysis. For a flat, planar electrode, the current response over time can be described by the Cottrell equation.

$$i = (nFAD^{1/2}C)/(\Pi^{1/2}t^{1/2}) \qquad 3\text{-}4$$

where, i is current (amperes), n is number of electrons per molecule (eq/mol), F, Faraday is constant (96,485C/eq), A is electrode area (cm^2), C is the concentration (mol/cm^3), D is diffusion coefficient (cm^2/s) and t is time.

This technique was applied for electropolymerizing the first layer of pyrrole polymer. A solution composed of pyrrole (10mM)/$LiClO_4$(100mM) was used to electropolymerize pyrrole on the surface of acid-washed electrode. The running voltage of 1.35 V was applied until a charge transfer of 30 mC is satisfied.

3-3-2-3. Differential pulse voltammetry

This technique is considered less accurate for measuring current peaks, as it is primarily used for characterizing the imprinted surface, rather than the precise quantification achieved through differential pulse voltammetry. DPV is known for its sensitivity and high accuracy.

DPV operates by superimposing small pulses onto a staircase waveform. It is applied to linear potential ramps, where short pulses (lasting 10–100 ms) with small amplitudes (1–100 mV) are used to generate fixed-magnitude pulses. During each pulse, the current is measured twice: first at the initial point (I_1) just before the pulse is applied, and then at the end of the pulse (I_2). The difference between these two current measurements ($\Delta I = I_2 - I_1$) is plotted against the potential to produce peak-shaped voltammograms, as shown in (Figure 3-6). In our work, Differential pulse voltammetry technique was implemented to showcase the capability of deposited MWCNT-APBA to form a reversible reaction with glucose and consequently create a non-conductive layer which inhibits charge transfer in the presence of a redox agent. DPV was conducted in a range of -0.2 - 0.6 V with a potential pulse of 50 mV and a pulse time of 50 ms.

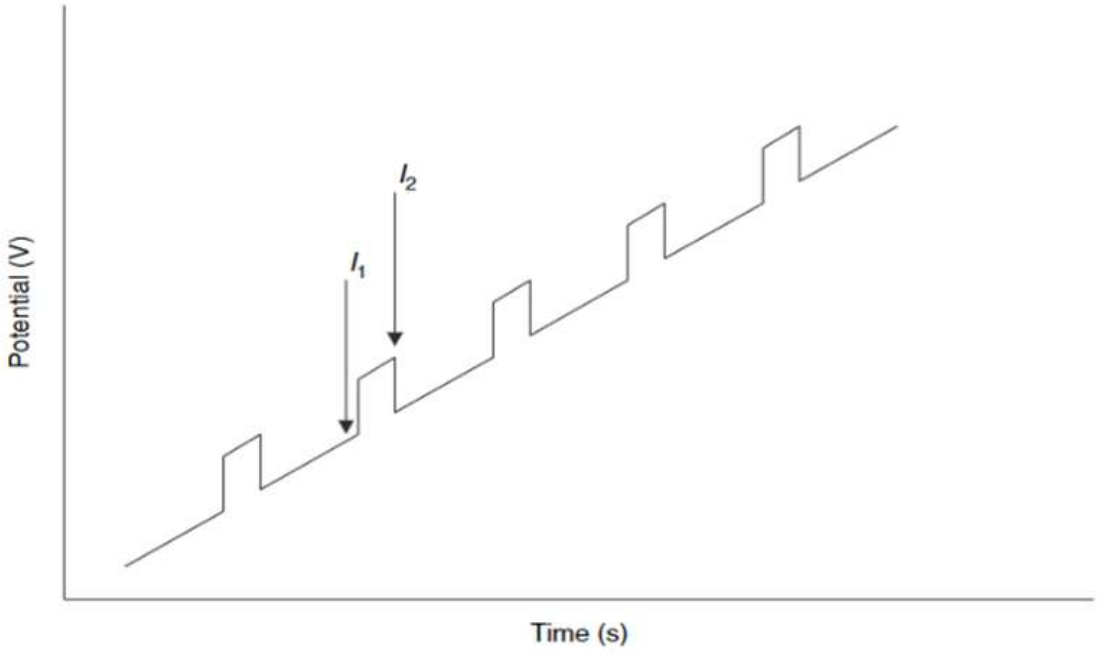

Figure 3-6 The differential pulse voltammetry mechanism [59]

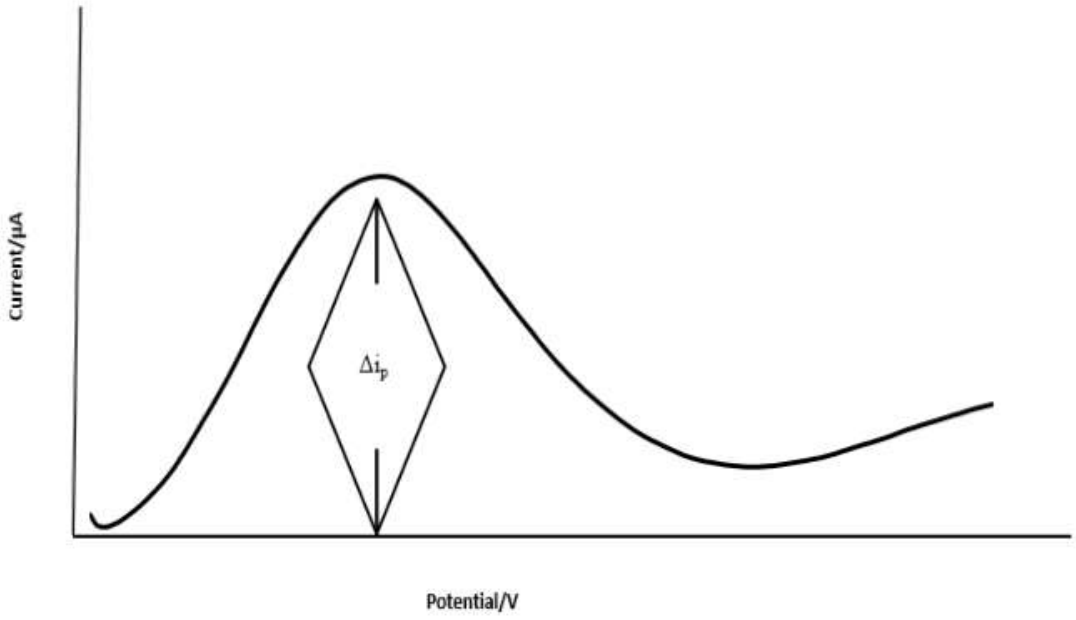

Figure 3-7 Typical response of a differential pulse voltammogram [59]

3-3-2-4- Square Wave Voltammetry

Square Wave Voltammetry (SWV) is a widely used electroanalytical technique valued for its high sensitivity and efficiency, making it particularly useful in many analytical applications. Here's a more detailed and approachable explanation:

SWV works by applying a series of alternating potential pulses on top of a staircase waveform. These pulses switch rapidly between a forward and reverse potential, allowing the system to capture a detailed current response. What makes SWV stand out is that it records the current at the end of each pulse—both forward and reverse—when non-Faradaic (background) processes have mostly settled. This ensures that the measurements focus primarily on the Faradaic (reaction-based) processes, which directly relate to the analyte (Figure 3-8).

In this work, square wave voltammetry were implemented to reveal that glucose's reaction with APBA is responsible for the reduction in faradic redox of $Fe(CN)_6$. This reduction will eventually

result in sensitive glucose detection. The SWV was operating under the voltage range of -0.2 V to 0.8 V at a step height of 3 mV, an amplitude of 15 mV, and a frequency of 20 Hz.

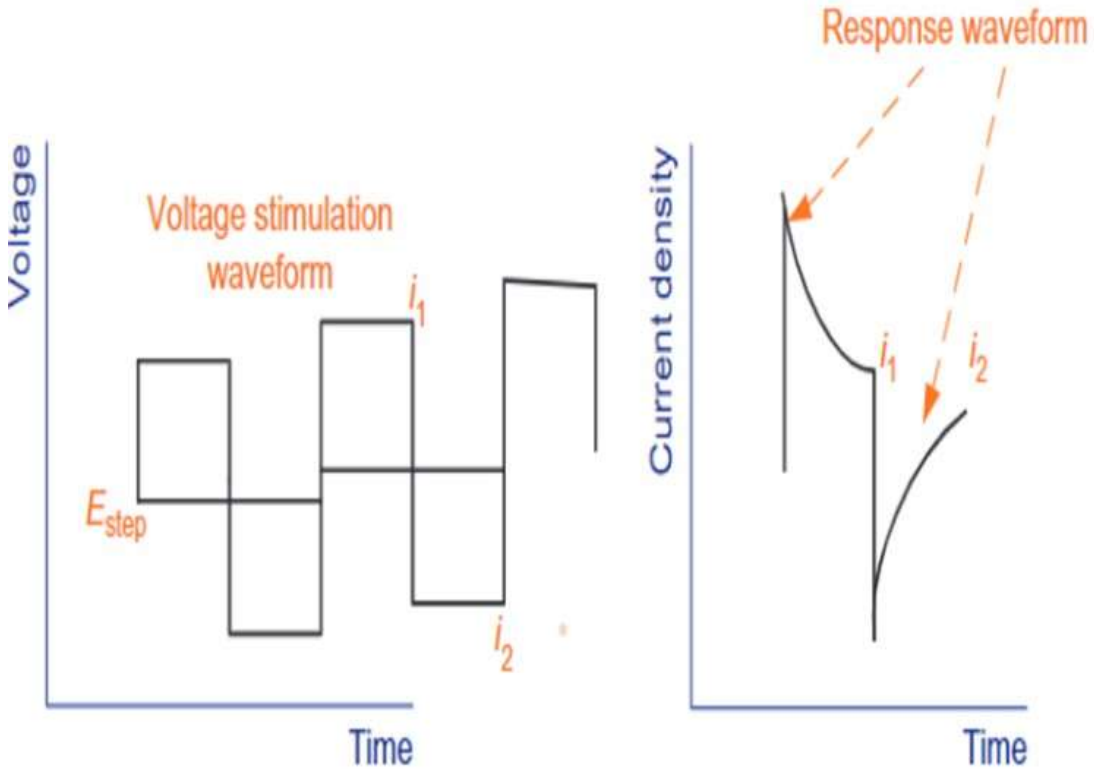

Figure 3-8 Square wave voltammetry waveform [60]

3-3-2-5- Electrochemical impedance spectroscopy

Electrochemical Impedance Spectroscopy is a powerful tool for studying what's happening on the surface of a working electrode. It can reveal important details like the electrode's stability, how fast reactions occur, and its double-layer capacitance, among other things. The process involves applying a small sinusoidal voltage—usually between 1 and 10 mV—on top of a steady baseline potential or the open-circuit potential. Any shifts in the phase or amplitude of this voltage create an alternating current (AC), which reflects changes taking place inside the electrochemical cell (Figure 3-9).

The impedance of the system depends on various factors, such as diffusion, protective layers, electron-transfer kinetics, and the resistance of the solution. Interestingly, the impact of these factors changes with frequency. For example, diffusion tends to dominate at lower frequencies, while electron-transfer kinetics take over at higher ones. What makes EIS so useful is its ability to measure over a wide range of frequencies, allowing you to detect multiple processes happening at different time scales—all in a single experiment.

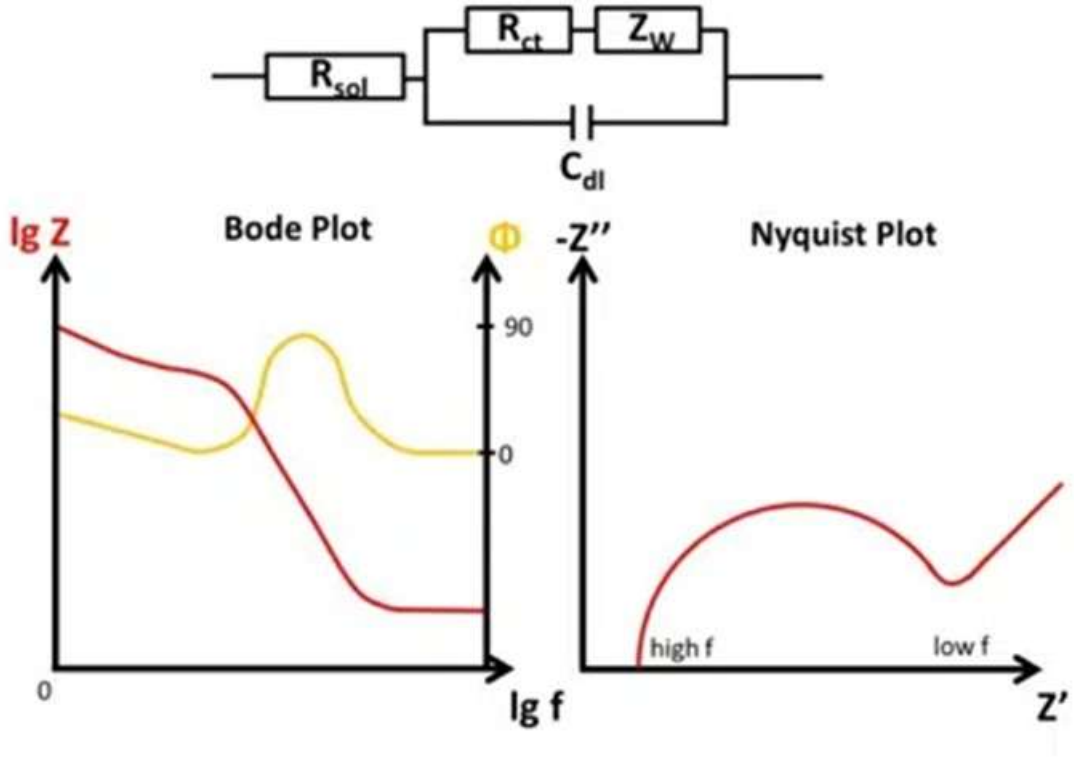

Figure 3-9 EIS of a Randles circuit including a Warburg element in a schematic Bode and Nyquist plot [60]

To investigate the charge transfer resistance of the polymer films, EIS measurements were performed. but in general, the polymer was allowed to stabilize for 5 seconds at either the open-circuit potential (OCP) or a fixed applied potential. This step ensured the system reached a steady state before starting the measurements (Figure 3-9).

A small voltage perturbation of 10 mV was applied to keep the system within a pseudo-linear range, and the frequency was varied from 100 kHz to 100 mHz during the measurements.

3-3-3-Characterization techniques

3-3-3-1- Scanning electron microscopy

Through the use of a focused beam of high-energy electrons from an electron microscope, various signals are produced on the surface of solid specimens. These signals, which come from interactions between the sample and electrons, reveal details about the sample's topography, chemical composition, crystalline structure, and orientation, in addition to its external appearance (such as texture). With magnification levels ranging from 20X to roughly 30,000X and a spatial resolution of 50 to 100 nm, this imaging method can cover areas with widths of approximately 1 cm to 5 microns. Specialized points on the sample can also be analyzed by the SEM, which is especially helpful for qualitative or semi-quantitative analyses of chemical compositions (using EDS) and crystalline structure and orientations (using Electron Backscatter Diffraction (EBSD)).

In this experiment, Hitachi S-4800 SEM within the Advanced Microscopy Facility at the University of Victoria was used to characterize the prepared MIP and NIP samples. In this analysis, samples were drop-casting onto a glass substrate and coated with gold and carbon for SEM and EDS, respectively, to increase conductivity. For imaging, the accelerating voltage was set to 5 kV, and working distances in the range of 8 mm and 15 mm were used. Subsequently, the acquired SEM images and EDS measurements were used to analyze the morphology and size distribution of the particles, using ImageJ software.

3-3-3-2- Raman spectroscopy

Raman spectroscopy is a scattering technique that involves the interaction of incident light with vibrating molecules, causing inelastic scattering. When a monochromatic laser illuminates a sample, most of the scattered light retains the same frequency as the incident light, known as Rayleigh (elastic) scattering [61]. A small portion, however, scatters at different frequencies, resulting in Raman scattering. If a photon relaxes to a higher energy state with a lower frequency than the incident light, Stokes lines appear on the Raman spectrum. In contrast, if the photon relaxes from a higher energy state with a higher frequency, anti-Stokes lines are observed. These processes, along with Rayleigh scattering, are key features of Raman spectra(Figure 3-10).

Raman spectroscopy provides a molecular fingerprint for identifying analytes and is non-destructive, making it broadly applicable. However, its sensitivity is limited due to the weak intensity of Raman scattering. In our project, Raman spectra was obtained under the following parameters: 532 nm laser, 5% laser power for 5 s for 2400 l/mm range. The Raman shifts were gathered in the range of 1000-2000 cm^{-1}.

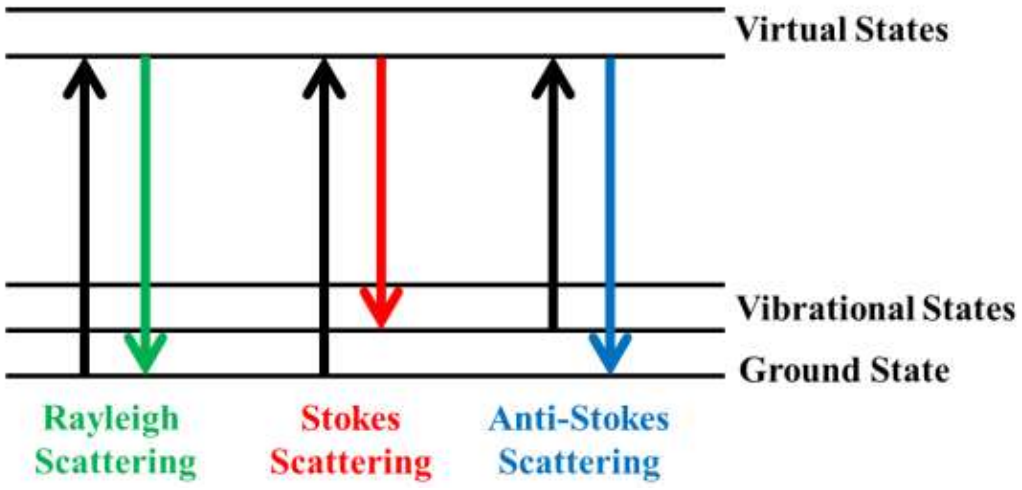

Figure 3-10 Different light scattering modes: Rayleigh, Stokes, and anti-Stokes scattering [61]

4. Results and Discussion

4-1. Steps to fabricating glucose sensor

4-1-1- Electro-cleaning of the electrode

Before functionalization, the screen-printed electrode (SPE) underwent electrochemical activation through CV in an aqueous solution of 0.05 M sulfuric acid (H_2SO_4). The potential was cycled between -2.0 V and +2.0 V vs. Ag Pseudo at a scan rate of 50 mV/s (**Figure 4-1**). This pre-treatment step plays a crucial role in removing surface-bound organic contaminants that may interfere with subsequent modifications and ensuring a clean, active surface for enhanced electrochemical responses.

The acidic environment facilitates the oxidation of organic impurities, while potential cycling promotes the renewal of the electrode surface, exposing more active sites for efficient redox reactions [62]. Additionally, this activation step helps to remove any insulating layers formed during storage or handling, thereby improving surface conductivity and electrochemical reproducibility [63]. This step also enhances the charge-transfer kinetics of the electrode by introducing hydroxyl groups on the surface [64].

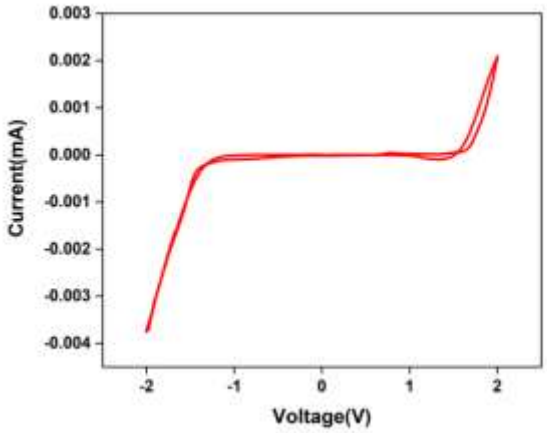

Figure 4-1 Electro-washing of SPCE

After electrode pretreatment, a PPy layer was deposited on the cleaned electrode surface through electropolymerization. Polypyrrole is a widely used conductive polymer in biosensor development due to its ease of synthesis, chemical stability, redox activity, and ion-selective properties, which make it effective in converting biological interactions into measurable electrical signals [65]. The overoxidation of PPy further improves its performance by introducing carbonyl and carboxyl functional groups into the polymer structure, enhancing its binding capacity for both positively and negatively charged species. These modifications contribute to the polymer's selectivity and sensitivity, particularly in MIP-based biosensors. Additionally, overoxidized PPy layers exhibit superior chemical and thermal stability, making them more robust and durable for practical sensing applications [66].

Consequently, a thin overoxidized PPy layer with a thickness of 8.5 μm was deposited on the electrode surface to provide a functional interface for the APBA-MWCNT composite, enhancing the sensor's sensitivity and performance. The electropolymerization was carried out by applying a constant potential of 1.35 V in a pyrrole (10 mM)/$LiClO_4$ (100 mM) solution at a slightly acidic pH (6.5) to ensure controlled film formation and stability (**Figure 4-2**)

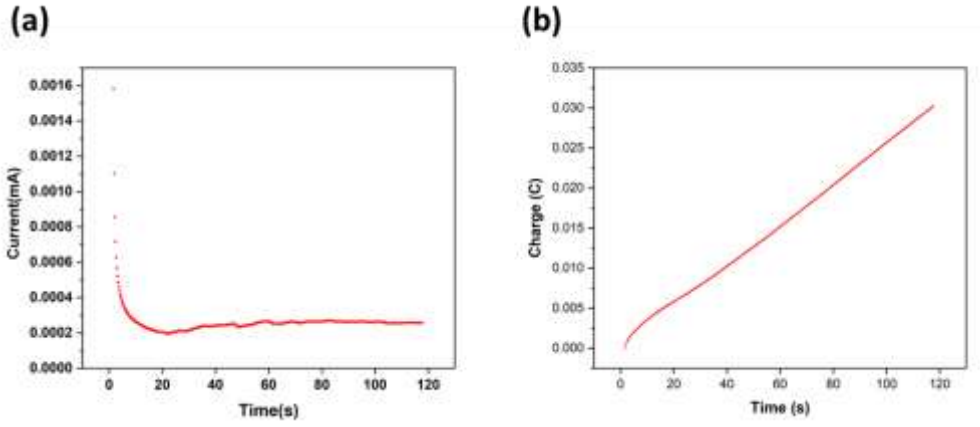

Figure 4-2 (a) current profile of electropolymerization at constant potential (b) Charge transfer profile of electropolymerization at constant potential

4-1-3- Deposition of recognition layer

The APBA-MWCNT composite possesses boronic acid groups capable of forming reversible covalent bonds with carbohydrates, particularly those containing 1,2- or 1,3-diols, such as glucose [67]. The formation of boronate esters affects the impedance characteristics of the electrode by altering the charge transfer upon glucose binding [68]. The glucose-boronic acid interaction is highly pH-dependent, with lower affinity at acidic pH due to boronic acids remaining protonated. In contrast, at neutral to slightly alkaline pH, boronic acids become deprotonated, enabling effective glucose binding [68, 69].

To ensure sufficient recognition sites for glucose in the MIP, a 10 µL layer of APBA-MWCNT composite was deposited on the polypyrrole surface. Prior to glucose introduction, the electrode was preconditioned in alkaline media to enhance the binding efficiency of the boronic acid groups.

4-1-4- Drop casting the template molecule

Next, a 50 µl of glucose (20 mM) was drop-casted on the surface of the modified electrode and incubated for 2 h at Ph=8, followed by washing off the unbounded glucose with PBS buffer. This protocol is, however, used for the fabrication of MIP sensor whereas in the NIP sensor this step was eliminated. The preconditioning step is done beforehand to ensure binding of glucose to boronic acid.

4-1-5- Formation of imprinting layer

A solution of PPy/APBA is used to electropolymerize a thin layer of polymer on the surface of the functionalized surface. This polymerization process has a striking effect in fabrication of imprinting glucose, as glucose is going to be trapped inside the polymeric matrix. The imprinting layer was fabricated by cyclic voltammetry under the optimized conditions in 0.01 M PBS (pH: 13). It is worth noting that the pH of the solution was adjusted by adding NaOH in the solution.

This Imprinting layer is thought to have a diameter in the nanometer scale. The $B(OH)_2$ of APBA polymer together with NH groups inside the imidazole ring of Pyrrole can form hydrogen bonds with the capped glucose. After the washing process is completed a vacant space analogous to glucose is left behind which enables sensitive detection of template glucose (**Figure4-3**).

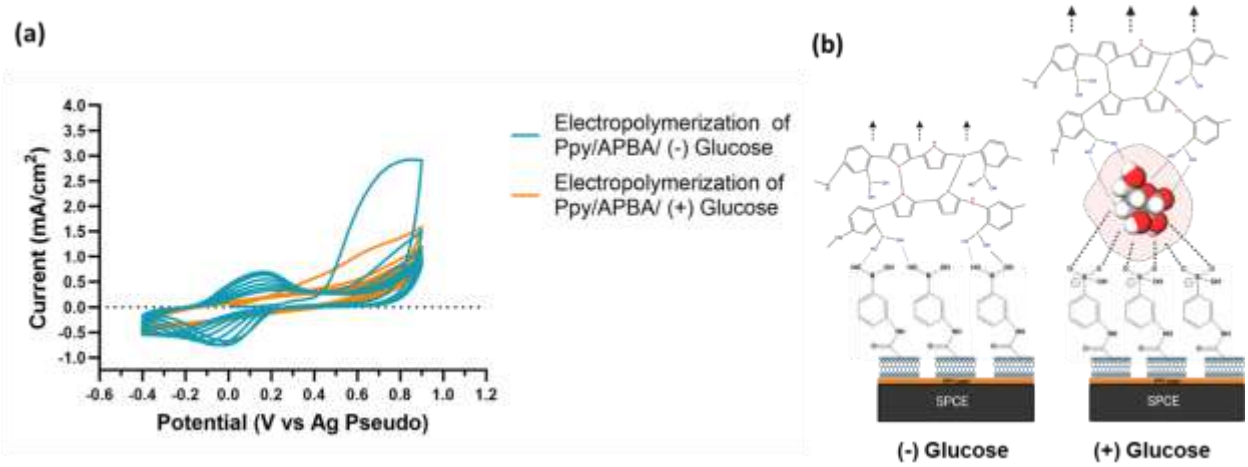

Figure 4-3 (a) Electropolymerization of PPy/ APBA imprinting layer in PBS (pH=13) under optimized conditions (b) Schematics of fabricated sensor with and without presence of glucose

4-1-6- Washing step

After synthesizing glucose-capped polymeric layer, the removal of glucose will attain molecularly imprinted layer which will be sensitive towards glucose. To accomplish the full removal of glucose from the sensor, the elution time has also been optimized. The appropriate solution is selected based on the low level of glucose binding affinity in the solution. As a result, solution of PBS (pH=3.5) was selected as the washing solution. Different parameters are affecting the detection of glucose in the imprinting layer, namely, the number of cycles, the concentration of APBA and the ratio of PPy to APBA. Given that the goal is to find the ideal conditions, DPV approach was employed to measure each peak's response. Because the imprinting sites inside the polymer matrix offers selective rebinding of the template, it is widely acceptable to investigate the template/monomer ratio regarding sensor's performance. This may also present an inhibiting

factor as the imprinted membrane may become increasingly thick and the current response was likewise affected when ratio was higher that 0.5. According to the (**Figure4-4**(e)), The higher amount of glucose did not yield a better result, which may be due to the altered electrokinetic reactions between APBA and glucose once the glucose concertation exceeds certain threshold [70]. The thickness of the layer is similarly attributed to number of cycles, which was discovered to produce optimum response when 8 cycles were run.

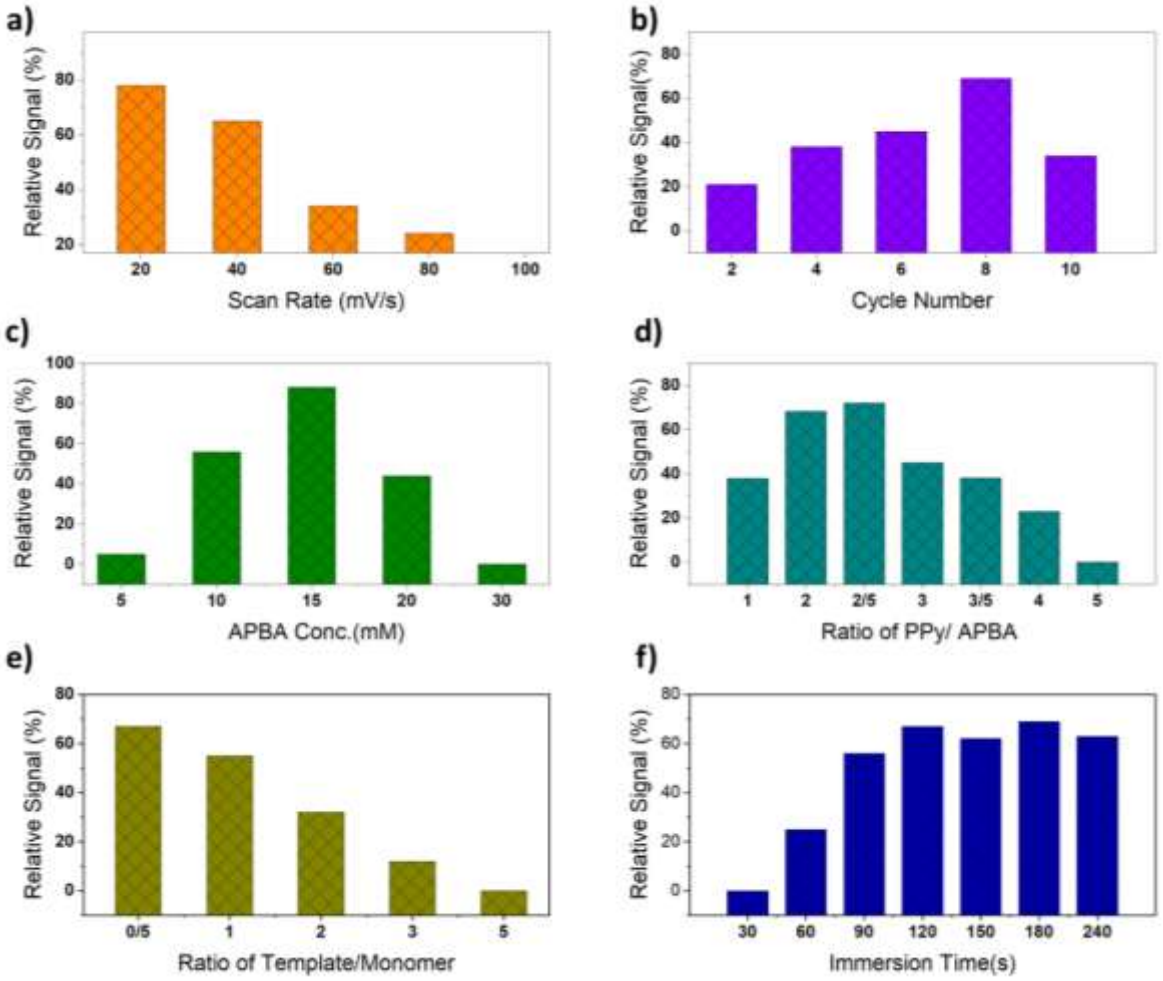

Figure 4-4 Sensor Optimization experiments for glucose recognition after the formation of imprinting layer: (a) scan rate of polymer deposition (b) number of cycles for imprinting layer electrodeposition (c) APBA concentration (d) Ratio of imprinting polymers (e) Ratio of Template/Monomer (f) Immersion time for glucose binding.

Additionally, the reason behind the reduction of the relative signal once the scan cycles went beyond 8 cycles is due to the production of less imprinting sites. Although, it may seem unrealistic,

due to the less availability of imprinted sites in a thick membrane, the binding capacity and kinetic will be affected and results in a poorer rebinding [71]. The immersion time for glucose binding has also been optimized, and since there is not much difference between the signals after 120 min, this time is chosen to be the optimal immersion time of the sensor.

Regarding the optimum scan rate, it also should be taken into consideration that really low scan rates lead to inhomogeneous deposition of the polymer, which could affect sensors response. We have witnessed this effect with regards to polymerization of at scan rate of 20 mV/s, as a result 40 mV/s was chosen as the optimal scan rate.

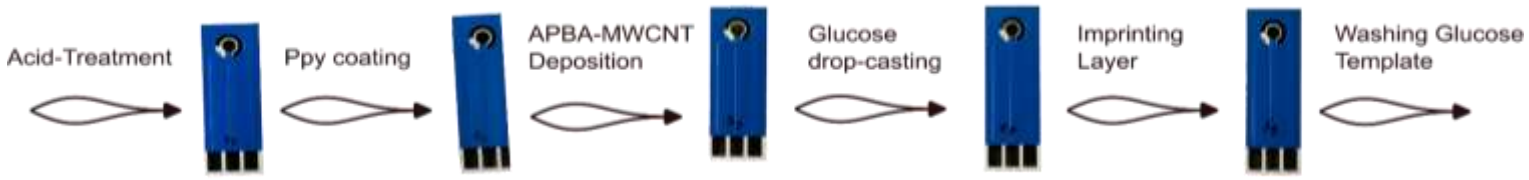

Figure 4-5 The sequential steps for fabricating Glucose MIP Sensor

In the **Figure 4-5** multi-step fabrication of MIP sensor has been shown. As discussed earlier each of these steps are optimized to achieve higher relative signal in the differential pulse voltammetry measurements. Indeed, the electrochemical and topographical characterizations are required to acknowledge the effect of each modification and better realizing the underlying effect of PPy coating, f-MWCNT and APBA-MWCNT modifications with respect to the bare sensor.

4-2. Material Characterizations

4-2-1- Scanning electron microscopy (FE-SEM)/ Energy dispersive X-ray (EDX)

In this section, we demonstrated the multi-step fabrication of MIP and NIP sensor. In figures below, the step-wise modification of sensor surface is shown (**Figure 4-6**).

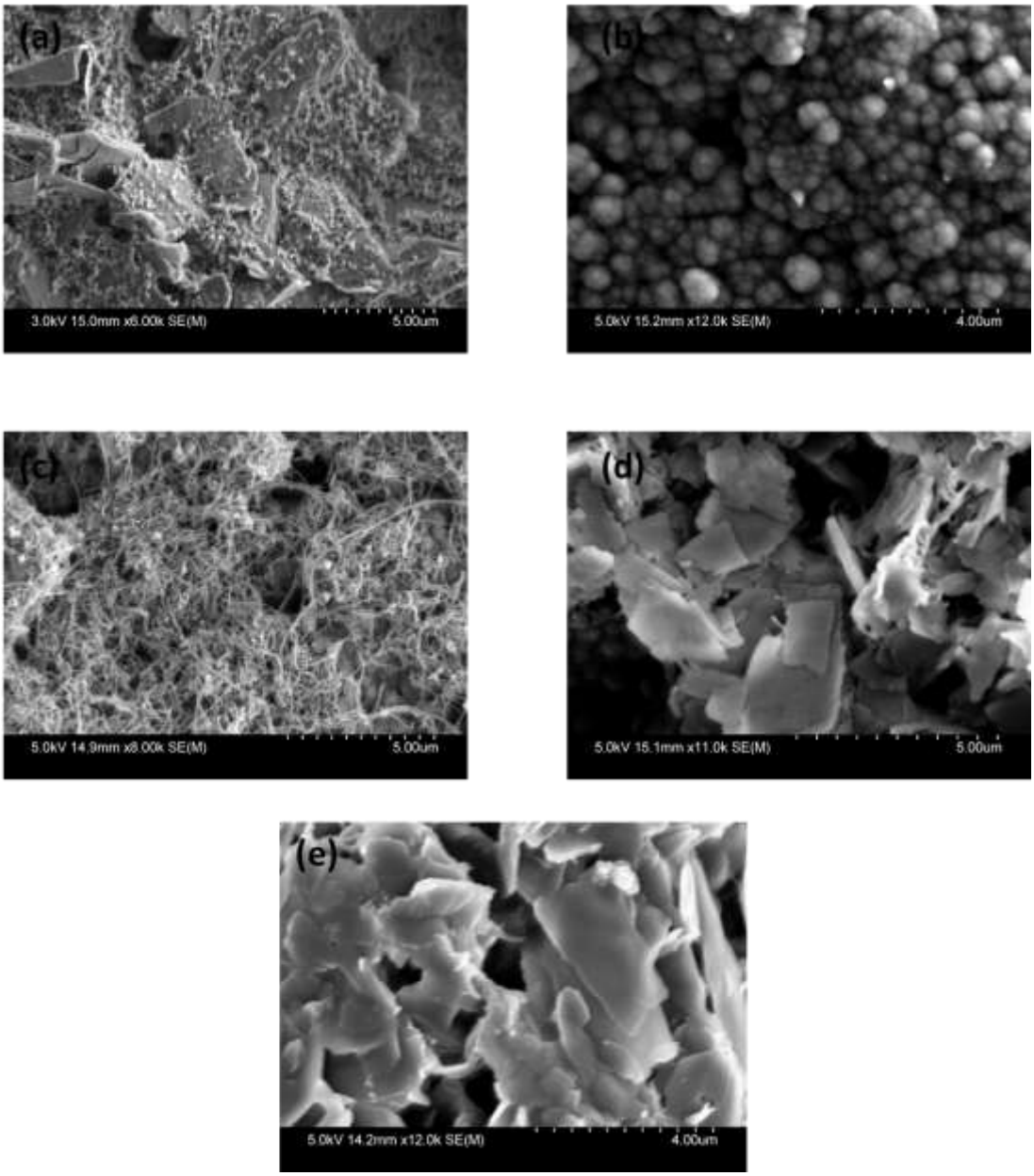

Figure 4-6 SEM images of multi-step Glucose sensor fabrication at × 11000 magnification. (a) Electrowashed electrode (b) Elecropolymerized pyrrole layer deposition (c) MWCNT drop-casting (d) APBA-MWCNT drop-casting (e) Glu immobilized onto APBA-MWCNT layer

Firstly, PPy is grown on the surface of pristine SPCE as suggested by [70]. The broccoli-shaped polymer makes up a layer with a diameter of around 7 μm on the surface. Next, f-MWCNT and APBA-MWCNT are sequentially shown, which proves the MWCNT composites will turn into planar shapes upon APBA polymer grown on the nanotubes surface. In addition, due to the lower

conductivity of the carbon electrode when the composite is deposited, the sample displayed a high charging effect. In addition, the EDS analysis revealed heightened peaks regarding different elements appearing during sensor fabrication steps. For example, the electro-washed carbon electrode revealed a sharp carbon peak (96.8%) whereas after the pyrrole layer is deposited the carbon excitation peak diminished and a Nitrogen (8.4%) peak starts appearing together with an unknown peak in 0.108 keV, which could be attributed to Lithium but cannot be confirmed. In addition, a sharp Cl peak (22%) is visible, which is related to the major effect of perchlorate in deposition of pyrrole monomer on the surface of the electrode. Furthermore, in the step 3 when carbon nanotubes are deposited onto the electrode, the atomic ratio of carbon material is increased from 50.1% to 64.7% while the Nitrogen peak starts to disappear again. There are also sign of elemental S and P peaks which can be speculated to come from the acid washing plus the using PBS to wash the debris on the electrode, respectively. The deposition of APBA-MWCNT could also be noticed by shadowing effects of the Cl. Plus, we can further speculate the imprinting layer could have a shadowing effect on the C composition in the fabricated electrode as well (Figure 4-7). The EDS mapping of imprinting layer also confirms incorporation of C (79.56%) into the recognition layer X-ray information still displays a high carbon composition. The spectra of N and C in the final imprinting layer is supposed to increase and decrease, respectively, as the composition of layer suggests. However, due to the fabrication of a very thin imprinting layer of polymer, the amount of the N element which is the significant part of pyrrole and APBA layer is negligible (**Figure 4-7**).

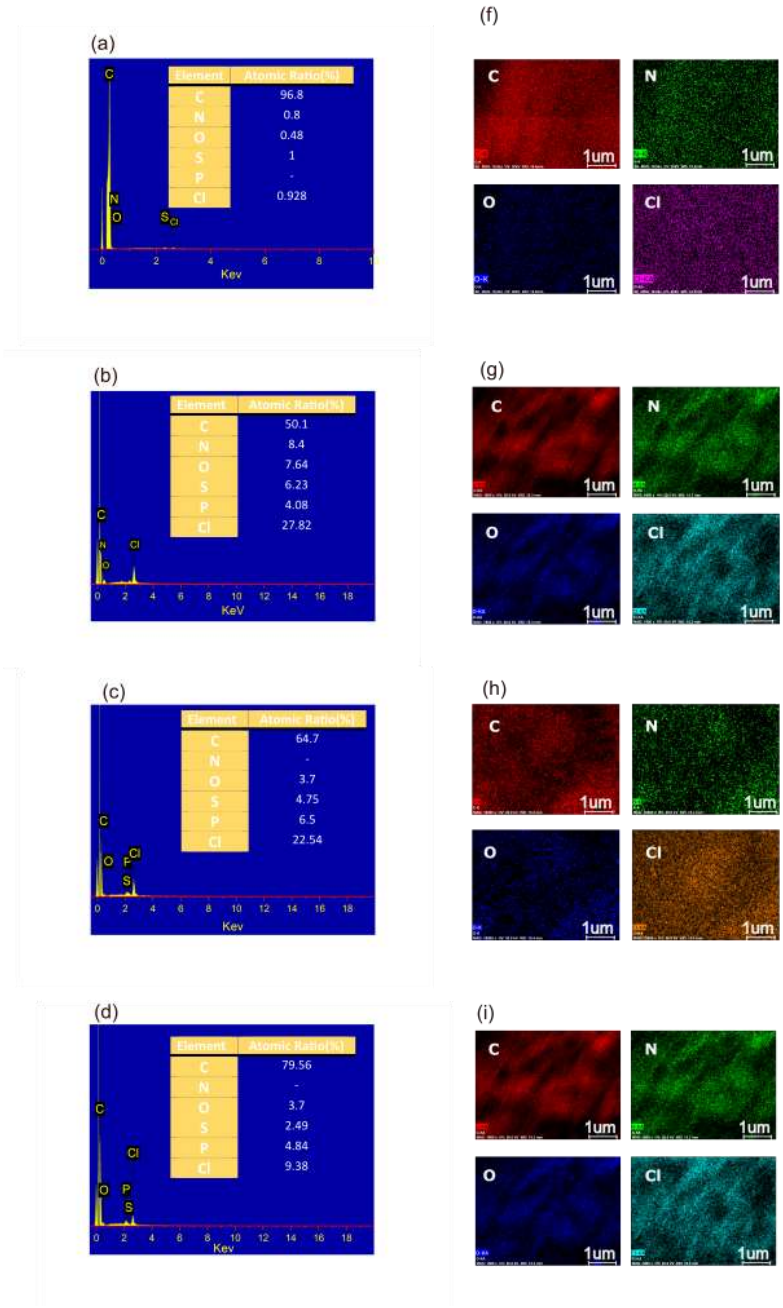

Figure 4-7 characterization of the sensor. EDS mappings for carbon (C), oxygen (O), nitrogen (N), chloride (Cl) of the sensor at different stages of preparation and the corresponding EDS spectra (a-d). (Bare carbon tri-electrode: Fig. (a),(f); after Pyrrol polymerization: Fig. (b), (g); after MWCNT deposition: Fig. (c), (h); deposition of MWCNT-APBA: Fig. (d), (i)

The spectra of N and C in the final imprinting layer is supposed to increase and decrease, respectively, as the composition of layer suggests. However, due to the fabrication of a very thin imprinting layer of polymer, the amount of the N element which is the significant part of pyrrole and APBA layer is negligible.

Figure 4-8 also compares the cross-section of the bare, PPy coated and final composite layer. The difference in diameters is not clearly noticeable, but with the first polymerization a thick layer of pyrrole is created. In this figure, however, the final composite sensor has smaller diameter than the PPy coated sensor, suggesting the imprinting layer's diameter is significantly smaller compared to the pyrrole layer. Additionally, it means that the second electropolymerization affects the morphology of the APBA-MWCNT drop-casted sensor. One other implication of this figure is the change in the morphology and conductivity of PPy. The NaOH treatment facilitates a counter anion exchange process where the intercalated anions (e.g., NO_3^-) in the PPy are exchanged for hydroxide ions (OH^-) [71, 72]. This is described in the study as a reversible process, where the conductivity of the PPy can significantly decrease due to this exchange, depending on the concentration of NaOH and the duration of treatment.

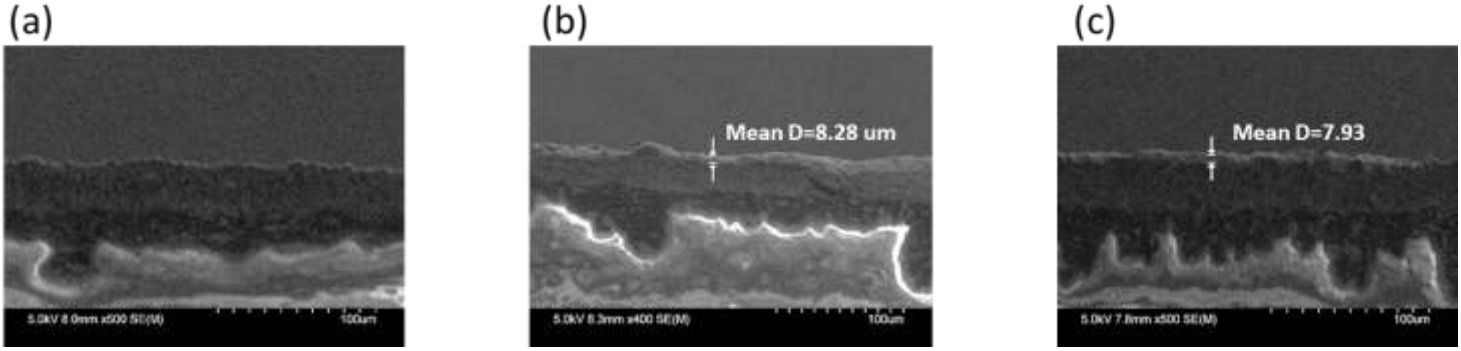

Figure 4-8 SEM characterization of film thickness (a) bare electrode (b) PPy-coated (8.28±0.5 µm) (c) Final composite layer (7.93±0.7µm). the film thickness were estimated by focusing on the cross-section of polymer film layer position on top of an angular stub. without gold coating.

4-2-2- Raman Spectroscopy

Raman spectroscopy is a versatile tool for characterizing carbon materials. Thus, each fabrication step was subjected to Raman characterization. In **Figure 4-9**, a clear disordered (D) band and a more pronounced graphite (G) band were observed at 1352.32 and 1580.08 cm^{-1}, respectively. Raman peaks associated with the D band is attributed to the breaking of sp^2 symmetry of carbon by the structural disorder and defects mostly due to the presence grain boundaries. Furthermore, the Raman peak in 1580.08 is attributed to the graphite defects arising from the stretching vibrations of the sp^2 carbon domains. After the overoxidized PPy deposition, Raman peaks in 1326.8 and 1587.5 cm^{-1} demonstrated intercyclic C-C stretching vibration mode, while the peak at 1411.66 cm^{-1} shows C-N stretching vibration, further acknowledging the integration of pyrrole polymer on the electrode (the highlighted area). The comparison between MWCNT and MWCNT-COOH revealed that the D-band's intensity was higher in MWCNT-COOH. The D-Band is attributed to the disorder in SP^3 Carbon, and the decrease in defect density or the structural homogeneity could be a major reason for its disorder. These defects can occur due to the alteration of the tube wall by functional groups. With regards to the APBA functionalization, a band appears on 1449 cm^{-1} which can represent both B-O symmetric stretching and C-C stretching vibration. The peak at 1180.04 cm^{-1} is also due to the B-C stretching mode. The glucose Raman spectra also give valuable information on 1075 cm^{-1}, 1109 cm^{-1} and 1201-1310 cm^{-1} which are widely associated with the CO stretching and COH bonds' bending mode, respectively.

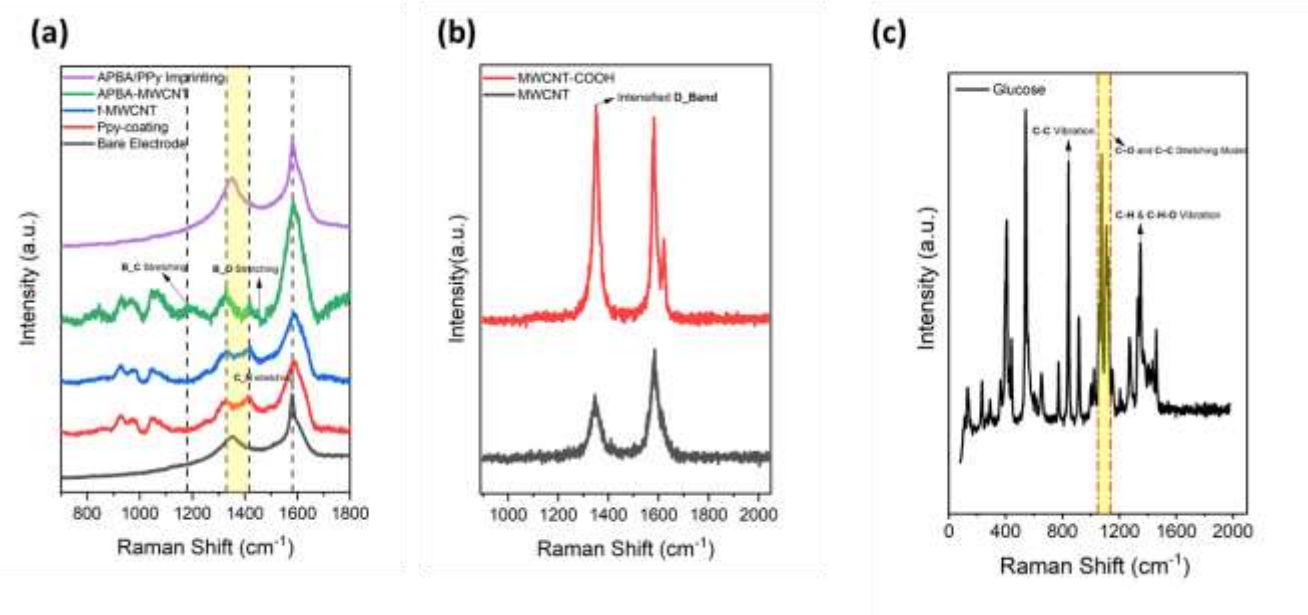

Figure 4-9 (a) Raman spectra of (a) layer-by-layer film modifications (b) MWCNT and MWCNT-COOH (c) 0.1 M glucose in dionized water

4-3- Electrochemical characterizations

4-3-1- CV and EIS characterizations

Each characterization step was investigated for indicating the peak current and the charge transfer resistance related to each modification.

Cyclic voltammetry analysis (**Figure 4-10**) revealed that the PPy coating resulted in an increase in current density by 0.44 mA/cm², indicating enhanced electrochemical activity on the modified electrode surface. Additionally, a positive shift in the oxidation peak potential from 0.14 V to 0.25 V was observed, reflecting alterations in the electron transfer kinetics at the electrode interface. Such a shift suggests that the PPy layer may either facilitate or impede the oxidation process depending on the interactions between the electrode surface and the analyte. Additionally, the PPy layer introduces new redox-active sites and improves the electrode's capacity to mediate electron transfer, resulting in the peak-to-peak current increase [73].

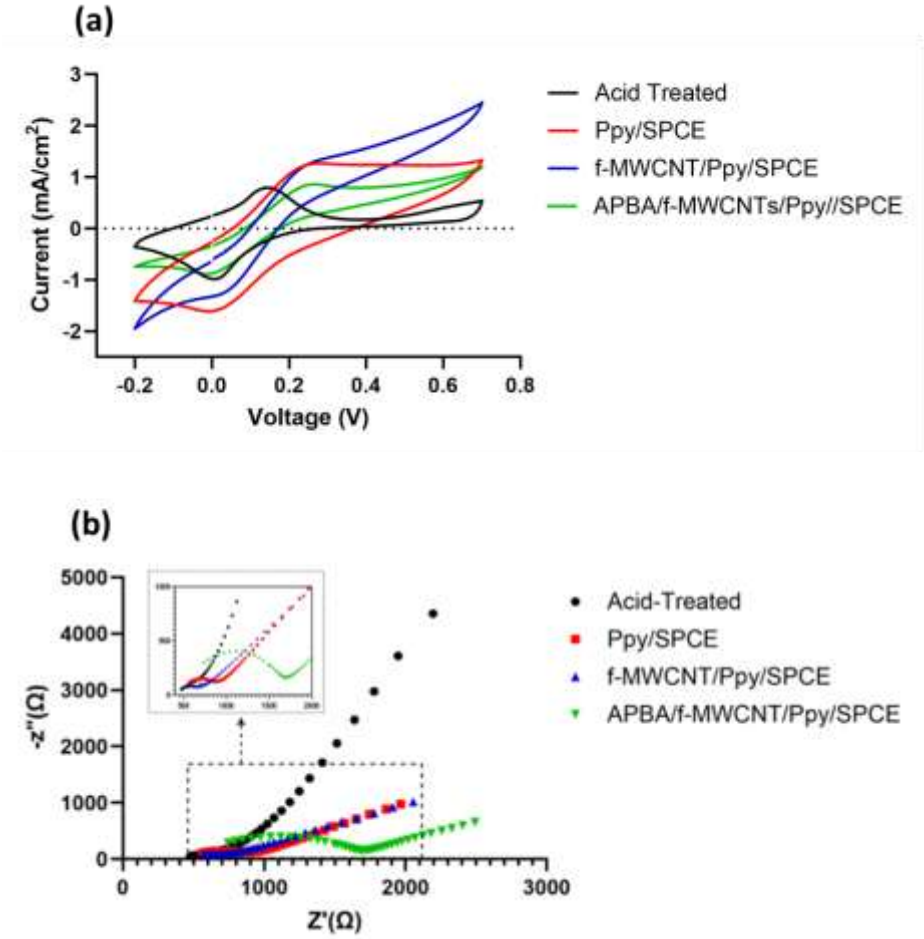

Figure 4-10 (a) CV characterization of developed sensor from Acid-treated to APBA/f-MWCNT modification (b) Electrochemical impedance spectra at Acid-treated, PPy/SPCE, f-MWCNT/SPCE and APBA/f-MWCNT/SPCE. Measurement were taken at room temperature with 2.5mM $Fe(CN)_6^{3-/4-}$(1:1)

Upon deposition of functionalized multi-walled carbon nanotubes (f-MWCNTs) on the electrode surface, the oxidation peak current remains relatively unchanged. However, the current continues to increase beyond the oxidation peak at 0.25 V, indicating enhanced redox kinetics due to the ability of f-MWCNTs to facilitate electron transfer between the electrode and the electroactive species [74]. This behavior is attributed to the high conductivity and large surface area of MWCNTs, which provide additional electron transfer pathways, improving the overall electrochemical performance [75]. Following the polymerization of APBA (APBA-MWCNT composite), a 0.4 mA/cm² reduction in peak current is observed, suggesting that the polymer layer

acts as a barrier to charge transfer. The EIS characterization further confirms these findings, showing a notable increase in charge transfer resistance (Rct) after the deposition of the APBA layer. This is consistent with previous studies, which highlight that the formation of PPy coatings introduces a charge transfer barrier, especially when overoxidation occurs during electrodeposition, reducing the polymer's conductivity [76, 77]. At high frequencies, the EIS results indicate a charge transfer-controlled regime, whereas at low frequencies, the electrochemical process is diffusion-controlled, where the diffusion of charge through the polymer layer dominates[78]. In this study, the PPy-coated electrode exhibited a charge transfer resistance of 64.36 $\Omega \cdot cm^2$ at 1000 Hz, a value that reflects the reduced conductivity due to the overoxidation of PPy, which forms carbonyl and carboxyl groups that impede electron flow.

Conversely, the addition of MWCNTs to the PPy layer significantly reduces the charge transfer resistance due to the high surface area of MWCNTs, which facilitate electron transfer and improve the electrode's conductivity. However, after the polymerization of APBA on the MWCNTs, the charge transfer resistance increases to 120.46 $\Omega \cdot cm^2$, indicating that APBA acts as a non-conductive layer. This behavior aligns with the inherent C, which lacks an extended π-conjugated system, thus limiting electron delocalization and increasing Rct.

Furthermore, the reversible reactions observed in the cyclic voltammetry analysis show a linear relationship between the square root of the anodic and cathodic peak currents, confirming that the system is diffusion-controlled [79]. The electroactive surface area was calculated using Equation 3.3, revealing that the APBA-MWCNT-modified electrode exhibits a significantly different electroactive area compared to the bare electrode, highlighting the impact of surface functionalization on electrochemical performance.

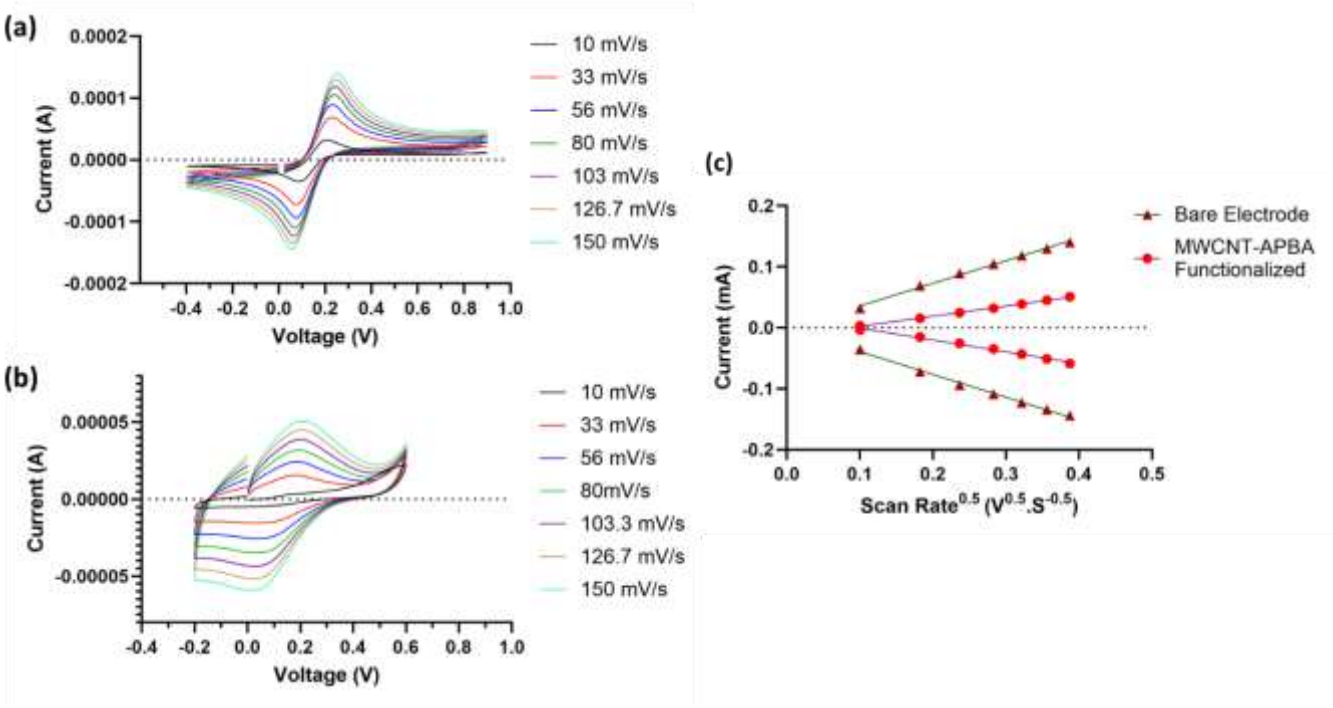

Figure 4-11 Cyclic voltammograms: the bare (a) and functionalized (b) SPCE under different scan rates (0.01->0.15) in 0.1M KCl+ 5 mM $Fe(CN)_6^{3-/4-}$ (c) the relationship between the anodic/cathodic current peaks of the redox mediator at the electrodes and the square root of the corresponding scan rates.

Based on the obtained results, the bare electrode shows larger electroactive area than the modified electrode, suggesting that APBA layer acts as an insulating layer that hinders the interfacial charge transfer, which was previously acknowledged by Nyquist plot of Figure 4-10. Based on the analysis, electroactive area of 0.110 mm^2 was observed for the bare electrode while the geometric area was 0.071mm^2 (**Figure 4-11**). After modification, the electroactive area was decreased to 0.04962 mm^2, and the functionalized electrode agree with the results obtained from **Figure 4-10**.

4-4- molecularly imprinted sensor platform

4-4-1- Developing Glucose-responsive system

The established APBA-MWCNT SPCE sensor was used for glucose immobilization. DPV and EIS results proved a reduced peak current and higher charge transfer resistance after glucose immobilization, respectively. This result proposes that polymerized boronic acids interacts with the diols from glucose molecules forming a saccharide nonconductive layer that blocks the charge

transfer between the $[Fe(CN)6]^{3-/4-}$ on the interface with the electrolytes. Surface-oxidized MWCNT facilitates the exposure of the boronic acid groups on the surface, which can, in turn, bind to cis 1,2 or 1,3 diols via covalent interactions to form five- or six-membered cyclic esters [80]. This interaction between PBA and glucose varies significantly across different pH levels due to the interaction between the boronic acid groups and glucose. Since the deprotonation of boronic acid groups occurs in alkaline condition, the binding affinity between APBA and glucose is enhanced, resulting in a stronger response (**Figure 4-12** (a)). The capability of boronic acids (BAs) to interact with saccharides presents huge potential in developing glucose-responsive sensors as presented by previous studies[81]. To determine the optimal pH for glucose sensing, the relative signal was calculated by using the current response of the acid-treated electrode as the reference, and comparing the signal intensities at various pH levels against this baseline current.

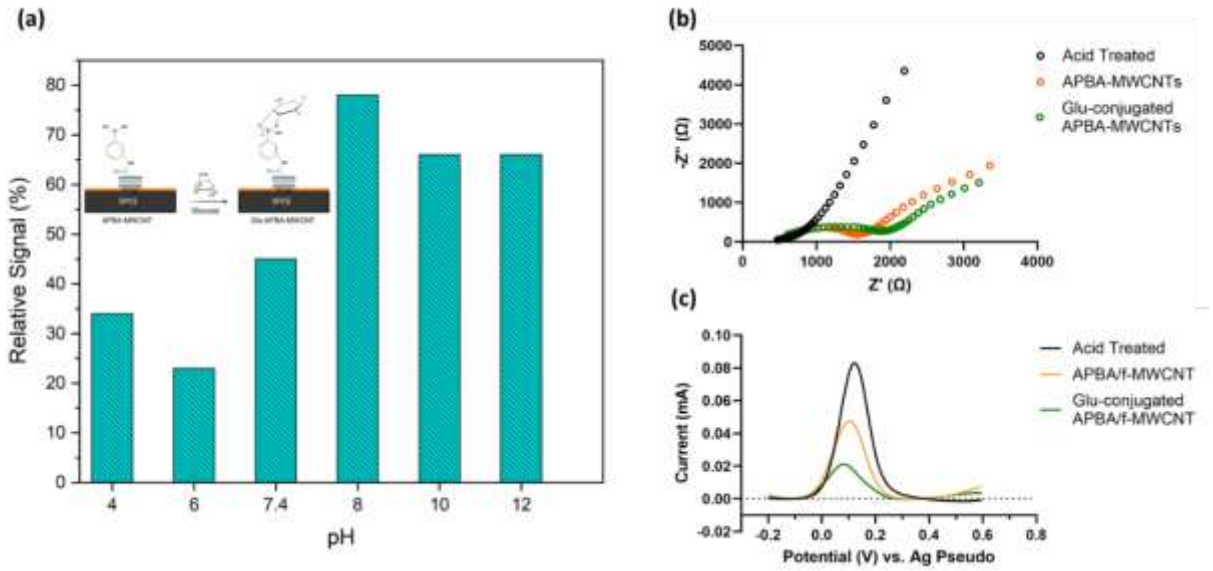

Figure 4-12 (a) finding optimum pH for glucose binding (b) Electrochemical Impedance spectra at APBA-MWCNTs/Ppy/SPCE and Glucose-bound/APBA-MWCNT/Ppy/SPCE (c) Differential pulse voltammetry of APBA-MWCNTs/Ppy/SPCE and Glucose-bound/APBA-MWCNT/Ppy/SPCE(Glucose concentration:10μM). Optimization for pH was done at 0.01 M PBS; EIS and DPV experiments were conducted in 2.5 mM $Fe(CN)_6^{3-/4-}$.

The optimized condition for the formation of boronate ester was found to occur at pH=8; it is noteworthy, however, that relative signal is relatively higher in alkaline conditions compared to

neural and acidic conditions. Upon glucose binding (**Figure 4-12**(a), (b)), we observed a 28 Ω.cm^2 change along with an apparent 26 µA drop in current. This observation is further backed up by the formation of a non-conductive layer [82]. the non-conductive film hindered the electron transfer of potassium ferricyanide, resulting in a sharp drop in the peak current [83].

4-4-2- Characterization of MIP and NIP sensors

One of the key steps in MIP sensor fabrication was optimizing parameters affecting glucose sensing performance. As shown in **Figure 4-13**, factors such as scan rate, cycle number, and polymer composition had a significant impact on sensor behavior. Based on the optimization, the final conditions for both MIP and NIP sensors were set at 8 cycles, a 40 mV/s scan rate, and a PPy/APBA ratio of 40:15 mM. The NIP sensor was fabricated under the same conditions but without glucose as a template.

The effect of PBS (pH 3.5) washing solution was also studied. The washing process reduced charge transfer resistance (Rct) for both sensors by removing loosely bound molecules from the electrode surface. However, the MIP sensor showed a higher Rct (6.52 kΩ) compared to the NIP sensor (5.82 kΩ) due to the presence of imprinted glucose molecules in the MIP, which hindered electron transfer between the redox probe and the polymer matrix. The complexity of the fabricated sensor requires a detailed look into the kinetics and diffusion characteristics of the sensors.

In the suggested equivalent circuit, Rs is the electrolytes resistance and two times constants were considered to signify multiple charge transfer kinetics of the imprinted sensor with a resistance R, the Rct, the constant phase elements CPE1 and CPE2 and the Warburg impedance W.

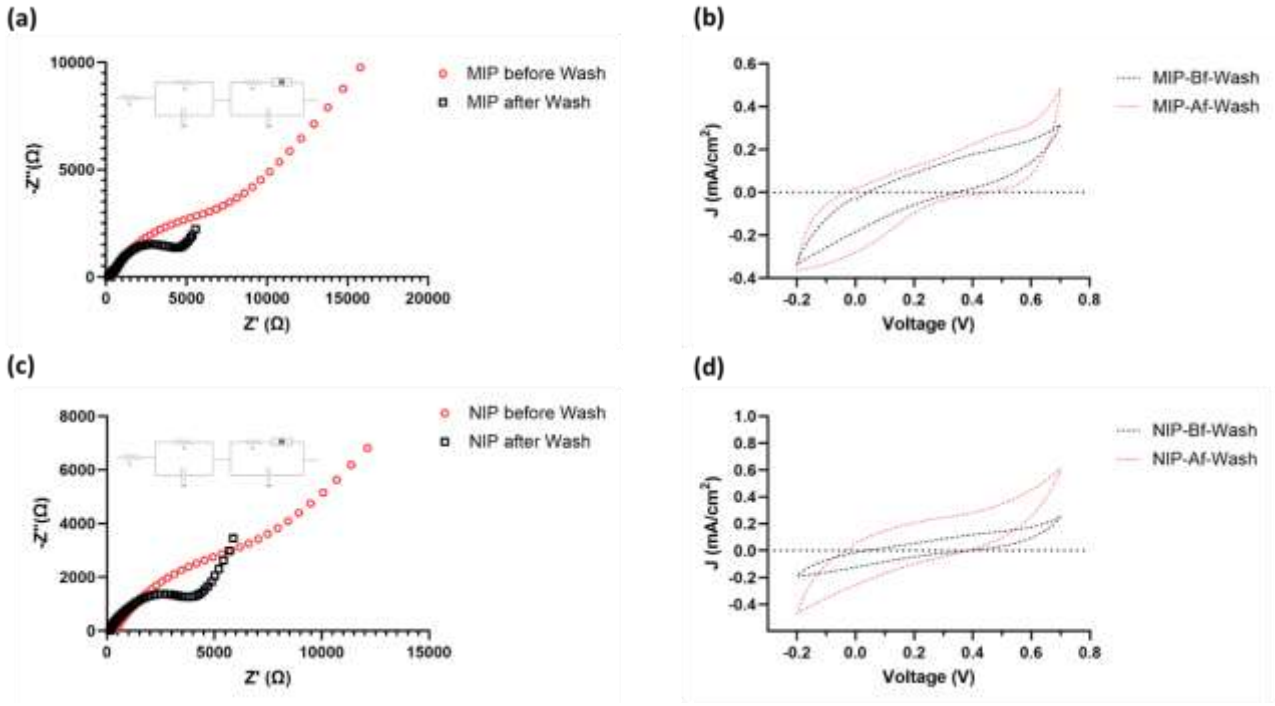

Figure 4-13 CV and EIS analysis of MIP and NIP (a,b) before and (c,d) after PBS washing

The elution of template was investigated in both NIP and MIP and gave an invaluable understanding of the performance of the sensor. Firstly, the charge transfer was improved for both NIP and MIP after the washing step; this is maybe due to the improved hydrophilicity of the APBA polymer when put in the acidic environment. The acidic environment can also boost protonation of amino groups in APBA and imprinting layer [80, 84]. Interestingly, the **Figure 4-14**(a) also revealed that it takes 180 min to wash the trapped template inside the polymer until there was no change in current caused by the change in glucose concentration. A rather fast change in current happens after 90 min of elution and that is when most of the template gets eliminated from the polymer bed causing the current to increase by approximately 10 µA, that shows the barrier for oxidation/reduction reaction is efficiently vanishing upon 90 min of wash. As a result, If given enough time, elution of template can result in polymer's swelling and solubility [80, 85, 86], and, in turn, the diffusion of redox probe will be facilitated. The second playing factor in removal of the template is that the boronic acid groups remain in its neutral form (-$B(OH)_2$), which is less

reactive and forms significantly weaker interactions with glucose in acidic environment and results in generating vacant sites withing the polymer network. In addition, the drop of R_{ct} from 6.52 kΩ to 3.18 kΩ can also be justified accordingly. this This is why NIP also experienced great conductivity restoration after washing step completed (**Figure 4-14** (a),(b)). The morphology changes caused by washing were shown for both MIP and NIP. There is a slight change of surface wettability as illustrated in Figure 4-14(c).

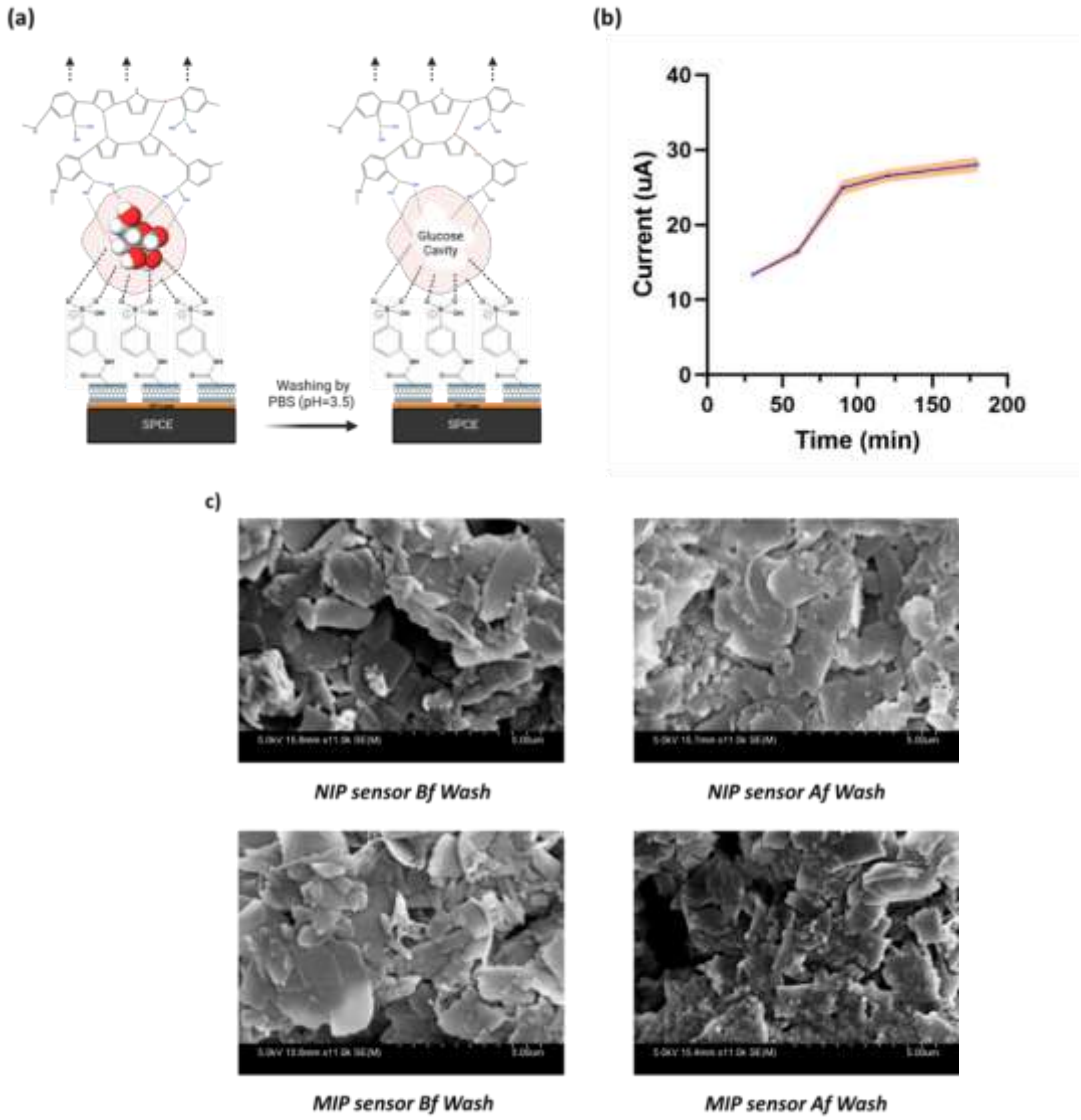

Figure 4-14 (a) Illustration of template removal mechanism (b) Effective elution time of glucose in PBS (pH=3.5) (c) SEM images of MIP and NIP before and after the elution.

CV experiments were performed in PBS buffer (pH=8) in order to identify the oxidation potential of glucose. The oxidation of glucose was detected to occur at 1.1 V at the second scan. This indicates that the glucose's oxidation shifts toward higher potentials in fairly basic environment which is due to the deprotonation of Glucose, altering its structure and making it less reactive towards oxidation. This structural change can increase the energy barrier for oxidation, shifting the oxidation potentials to higher values[31]. In our investigation of glucose electrooxidation, , we also examined the nature of electrooxidation of glucose. Given that chronoamperometry measurements of glucose ranging from 0.1 to 1 mM at a constant potential of 1.1 V vs. Ag Pseudo was performed, the increase in concentration of glucose draws a similar association with the increase in anodic currents. Based on the obtained results, the average diffusion coefficient of glucose was calculated to be $5.6 \times 10^{-6}\ cm^2\ s^{-1}$ by the Cottrell equation (3-4). **Figure 4-15** (b) clearly points out to the relationship between the current and reverse square of time after the current was stabilized. In the equation, I is the current (A), n is the number of the electrons transferred, A is the electroactive surface area of the electrode (cm^2), D is the diffusion coefficient ($cm^2 s^{-1}$), C is the concentration of the glucose (mol cm^{-3}), and t is the time elapsed (s).

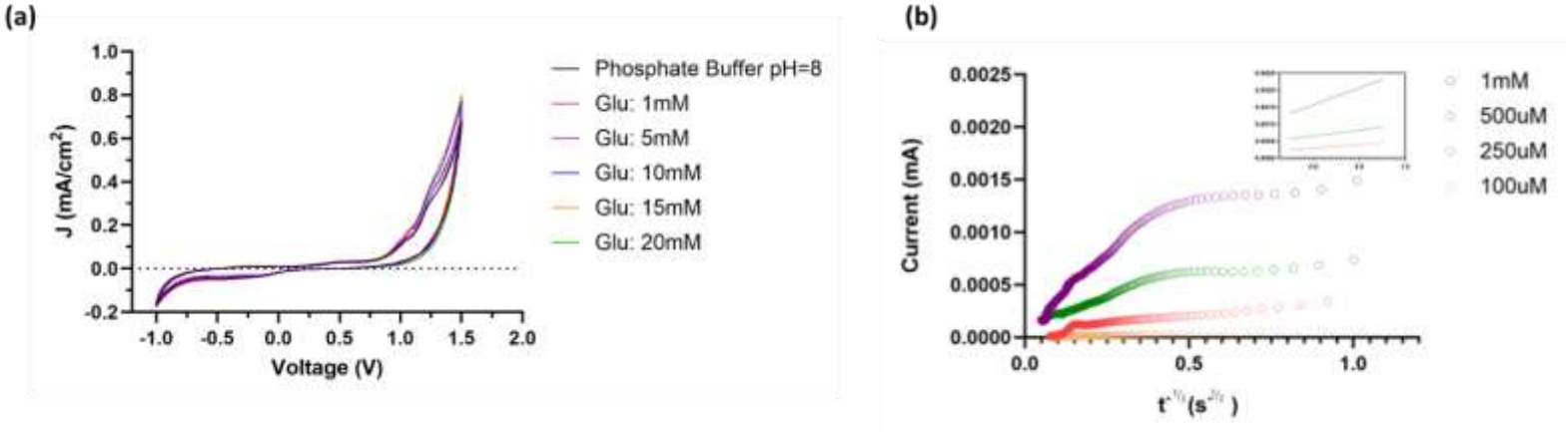

Figure 4-15 (a) Electrochemistry of glucose in -1v_1.5v range for 100 $^{mv}/_{s}$ and 2 cycles in PBS at pH=8 (b) Chronoamperometry measurements recorded at applied potential of 1.1 v for MIP in 0.1 mol L^{-1} PBS (pH 8) with different concentrations of glucose from 0.1 to 1 mol L^{-1}.

4-4-3- Analytical performance of MIP sensor

The performance of the MIP sensor was evaluated across different glucose concentrations in PBS buffer (pH 8) using SWV. The measurements were conducted in the presence of a redox probe solution, and the corresponding currents were recorded. The SWV results demonstrated the sensitivity of the MIP sensor to glucose concentration changes, with peak signals appearing at approximately 0.15 V (**Figure 4-16**). To assess the differences between the bare electrode, MIP, and NIP sensors, their current responses were compared. As expected, the bare electrode exhibited the highest current signal since the redox marker had unrestricted access to the electrode surface, facilitating efficient electron transfer. In contrast, the NIP sensor showed a significant reduction in current, indicating that the polymer layer acted as a barrier that prevented the redox probe from reaching the electrode surface. After the removal of glucose from the MIP sensor, the current partially recovered, suggesting improved electron transfer. However, the increase in current was limited, indicating insufficient vacant binding sites for glucose rebinding [87, 88]. One possible reason for this limited improvement is the second polymerization step on the glucose-bonded APBA layer, which may have replaced the bound glucose molecules with polymer monomers, thus reducing the number of available binding sites for glucose rebinding. This could explain the narrow linear detection range of the sensor, as fewer vacant cavities were available for glucose capture[89]. Upon introducing glucose into the MIP sensor, the current decreased steadily, confirming that the reduction in oxidation current was caused by glucose rebinding rather than interference from the redox marker. Furthermore, the SWV results indicated that the MIP cavities reached saturation after loading 10 µM glucose, suggesting that only a limited number of active binding sites remained available.

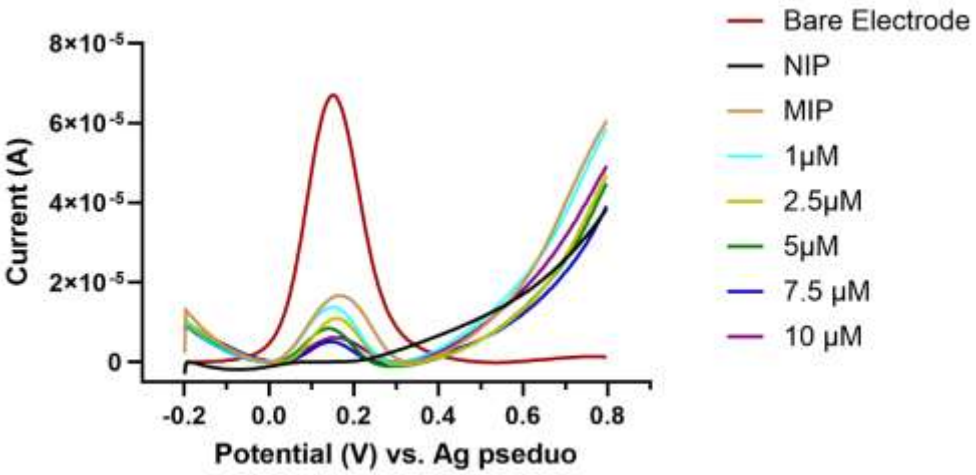

Figure 4-16 Square wave voltammograms recorded for the concentration dependent detection of glucose in PBS (pH=8). SWV measurements were conducted at room temperature with 5mM Fe(CN)63-/4- in 0.1 KCl

Impedance spectroscopy was the chosen method to sensitively detect the glucose molecules. MIP and NIP sensors were compared in terms of their capability to entrap glucose molecules, and regression analysis were carried out in concentration range of 1-20 μM. As Figure 4-13 describes the Randle equivalent circuit used to fit EIS analysis, R_{ct} values were driven from the Nyquist plots. As exhibited, the Rct values are increasing with the increase in the concentration of glucose. Upon immersing the MIP sensor in the target solution for 120 min, the boronic acid groups form gluco-boronate ester in contact with glucose, leading to introduction of a negatively charged boronate ester inside the polymeric matrix. Consequently, the negatively charged redox marker is further getting pushed away when the concentration of glucose increases, triggering larger changes in the charge transfer resistance of the sensor [90]. The NIP sensor was not responsive to the change in different concentration of glucose as illustrated in **Figure 4-16**. However, upon introduction of the glucose to NIP sensor a change in charge transfer were observed which could be attributed to the accumulation of the glucose on the surface or random cavities (Rct: 1220 Ω). This idea is further proved when the sensor was not responsive to the further increase in glucose

concentration. In the presence of imprinted cavities, the Rct increases linearly with the concentration of glucose.

Since the cavities of the MIP sensor were filled, the R_{ct} increased due to blocked electron transfer process, leading to a larger semi-circle in the Nyquist plots with gradually increased glucose concentration. When the concentration of glucose exceeded 20 µM, no more change in R_{ct} were observed suggesting the saturation of template molecules within the polymer matrix. The regression equation is $R_{ct} = 28.12 \times [Glu] + 764.5$ with $R^2 = 0.94$. From the Nyquist plots, the LOD and LOQ were obtained to be 6 and 18.16, respectively (**Figure 4-17**).

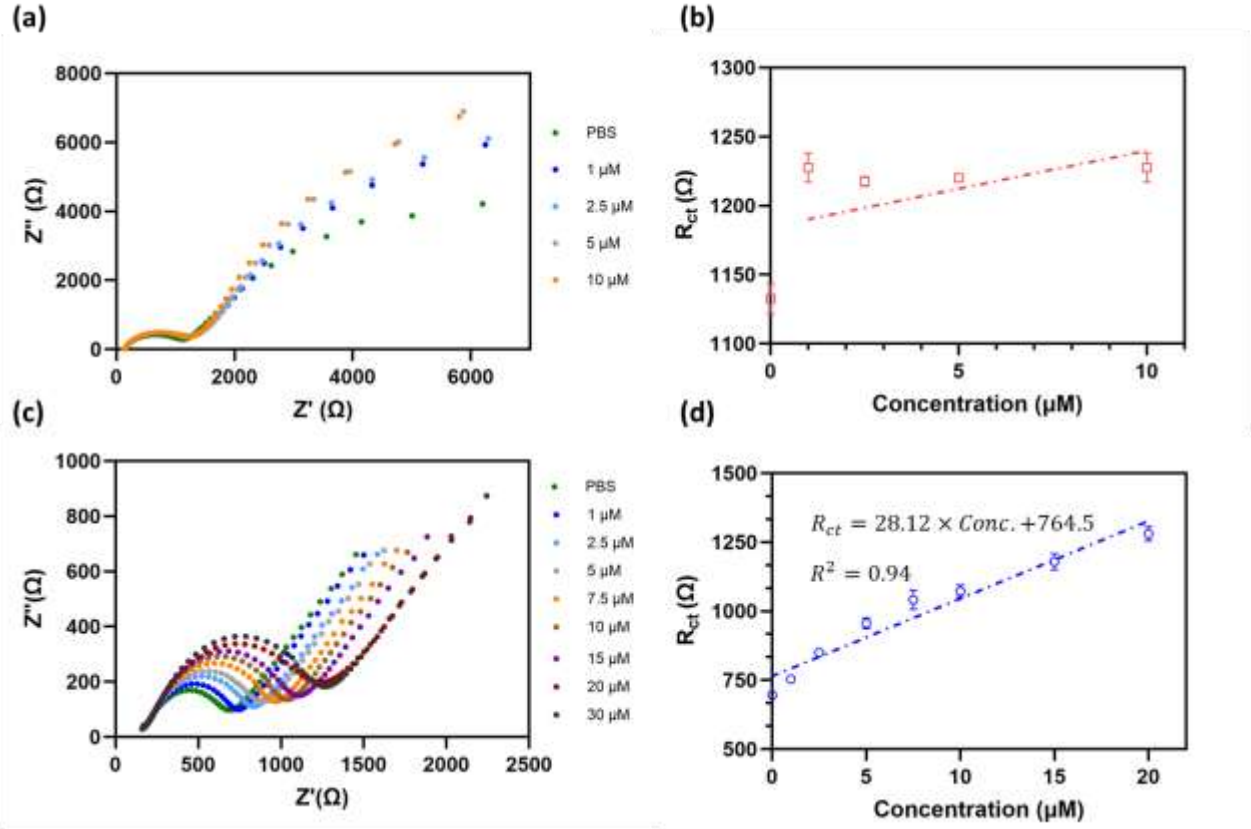

Figure 4-17 Electrochemical impedance spectra obtained for MIP(c&d) and NIP(a&b) sensor for concentration dependant detection of glucose in PBS (pH=8). EIS experiments were conducted in 0.1 M PBS containing 5 mM $Fe(CN)_6^{3-/4-}$

4-4-5- Interference study

The selectivity of the developed glucose sensor was evaluated using electrochemical impedance spectroscopy. The influence of ascorbic acid (Vitamin C), a common interferent, was assessed for the MIP sandwich-type sensor by incubating it in a 5 µM solution of the interfering substance prepared in 0.1 M PBS at pH 8. Given that Vitamin C is present in physiological fluids at concentrations comparable to glucose and exhibits similar redox properties, its potential to interfere with electrochemical glucose detection was carefully examined [91]. The interferent was analyzed both individually and in combination with glucose to simulate physiological conditions. The observed changes in charge transfer resistance (ΔR_{ct}) before and after incubation with the interferent and glucose are presented in **Figure 4-18**. Notably, the ΔR_{ct} value for ascorbic acid (603 Ω) was significantly lower than that for glucose (1141 Ω), highlighting the sensor's specificity toward glucose. These results confirm that the MIP sensor effectively distinguishes glucose from interfering species, maintaining selective recognition even in the presence of high concentrations of ascorbic acid.

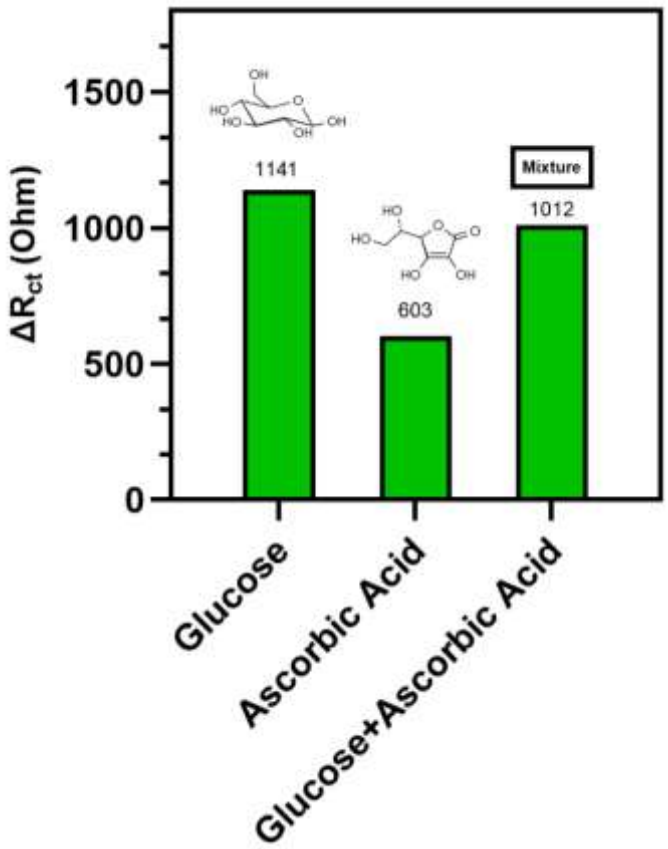

Figure 4-18 Interference study of ascorbic acid

4-4-6- Sensor stability and reusability

The stability of the fabricated MIP sensor was evaluated over 30 days using two identical sensors. The sensor maintained a consistent signal for up to 15 days, with a deviation of only 0.5% between the two sensors during this period. However, after 15 days, the signal stability decreased, resulting in a deviation of 4.6% between the sensors. Despite this decline, the sensor demonstrated excellent stability for 15 days (**Figure 4-19**(a)), showcasing its potential for widespread applications in sensing technologies. The degradation of signal stability after 15 days may be attributed to the hydrophilic nature of ClO_4^--doped polymers, which could lead to polymer swelling and solubility issues over time [88].

The sensor's reusability was also promising, as the signal remained consistent before and after washing steps. When exposed to 10 µM glucose solution and subsequently washed, an approximate 10 µA current change was observed. The consistence changes in current exhibits MIP's potential in successful rebinding of glucose up to tenth repeat, with sensor's response remaining at the same level. This acknowledges the impedance MIP sensor is inherently sensitive toward glucose concentration change. It is also noteworthy that no desquamation of the film was witnessed as a result of constant washing of the sensor in the tenth repeat [92]. This consistent performance highlights the MIP sensor's capability for use in reusable sensing applications, reinforcing its practicality for cost-effective and sustainable diagnostic kits.

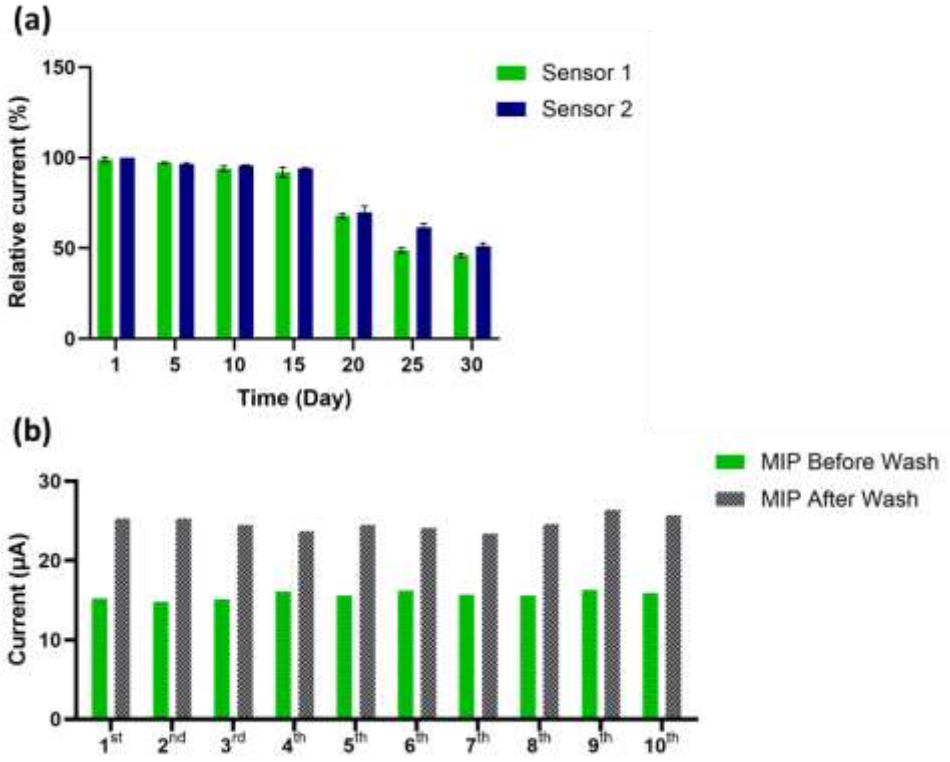

Figure 4-19 (a) Stability of Sandwich-MIP sensor over a period of 30 days (b) peak current of glucose after glucose elution and rebinding from 1st time to 10st time. Glucose concentration: 10µM

Table_4-1 presents the performance of MIP-based glucose sensors from the literature. Our multi-layer sensor preparation method offers high sensitivity, with acceptable linear range and high stability. The comparison between NIP and MIP revealed the successful fabrication of glucose cavities, which ultimate in remarkable sensing performance of MIP sensor. The optimization of polymerization parameters has an immense effect on the successful fabrication of a sensitive sensor. Afterwards, the conjugation pH of glucose and elution time of glucose are also important parameters that differentiates the capability of a MIP sensor against a NIP sensor. Furthermore, the incorporation of glucose binding moiety inside the MIP matrix with a pH-responsive conjugation offers a huge potential in fabrication of highly reusable glucose kits.

Table 4-1 Comparisons of the sensing performance for the MIP-based electrochemical sensors for glucose detection.

MIP sensor	**Polymerization method**	**Read-out technology**	**Linear range(mM)**	**stability**	**LOD (µM)**	**Ref.**
GA/AAM/EGDM immobilized onto Al-PVC substrate	Thermal Polymerization	Heat-transfer Method (HTM)	0.0194−0.330	---	19.4	[93]
BA-based MIP/GCE	Electro-polymerization	Potentiometry (PT)	0.75-18	1 week (PBS, r.t., 90%)	230	[94]
MIP/CuCo/SPCE	Electro-polymerization	Chronoamperometry (CA)	1-25	---	600	[95]
molecularly imprinted polymeric micelle(MIPMs)	Photopolymerization	Cyclic Voltammetry (CV)	0.2-8	30 days, tested every 1 week	50	[96]
Sandwich-type BA-functionalized MIP/SPCE	Electro-polymerization	Electrochemical Impedance Spectroscopy (EIS)	0.001-0.02	15 days, 2 replicates for each sensor	6	This work

5. Conclusion & Future work

5-1. Summary

This study involved the comprehensive material and electrochemical characterizations of multilayer BA-functionalized MIP sensor. The step-by-step fabrication of sensor included the pre-treatment, electro-polymerization of PPy conductive polymer, drop-casting functionalized recognition layer, and after the template deposition, the electro-polymerization of imprinting layer constructs the sandwich-type sensor.

The parameters essential for intact imprinting of glucose inside polymeric matrix were investigated by differential pulse voltammetry; i.e. n number of cycles, scan rate (mV/s), ratio of polymer composition, template/polymer ratio and immersion time. The optimized parameters were 8 cycles, scan rate of 40 mv/s, 2.5 PPy/APBA, 2.5 template/monomer and 120 min immersion time, respectively. The SEM characterization of sensors surface together with energy dispersive X-rays proved the successful fabrication of multi-layer sensor. The broccoli-shaped appearance of polymer indicated the successful fabrication of electroconductive layer with an 8.4% atomic ratio of Nitrogen. With carbon-nanotubes deposition the carbon composition increased from 50.1% to 64.7%, which also agreed with the SEM images. Raman spectroscopy also revealed successful fabrication of MWCNT-COOH with an intensified D-band. Furthermore, Raman bands for stepwise layer-by-layer functionalization accurately corresponded to each layer modification, and the diameter of pyrrole thin layer and final composition were 8.28 and 7.93 µM, respectively. Electrochemical analysis of each layer was done by EIS and CV methods. This study finds out that PPy thin layer and MWCNT-APBA deposition induced a charge transfer resistance of 64.36 $\Omega \cdot cm^2$ and 120.46 $\Omega \cdot cm^2$, respectively. A study of Randle-Sevic analysis of bare and functionalized electrode found out an electroactive area of 0.11 mm^2 and 0.04962 $mm^{2,}$ respectively. The contributions of this sandwich-type molecularly imprinted platform were listed as below:

- The effect of template attachment onto the BA moieties of recognition layer was assessed both by EIS and DPV
- The suitable pH for conjugation of Glucose to boronic groups in the recognition layer was optimized.
- The charge transfer resistance of MIP and NIP sensors were investigated before and after the elution process. Furthermore, the EIS data were also modelled to appropriate equivalent circuit model.
- Effective elution of glucose was also experimented to occur at 180 min, and the material characterization of MIP and NIP before and after elution was obtained.
- The diffusion coefficient of Glucose was acquired through analyzing the electrochemistry of the Glucose.
- This MIP-based sensor presents a cost-effective platform with the potential for repeated use, enabling reusable sensing capabilities within a single device. Furthermore, owing to the sensor's high selectivity, this class of sensors can deliver stable and reliable signals for target bioanalytes, demonstrating strong sensitivity toward the molecule of interest even in complex real biological matrices such as sweat, saliva, or blood.
- SWV and EIS were adopted to quantify the efficiency of MIP and NIP sensors in detecting low amount of glucose in physiological environment.

5.2- Future Work

While this thesis has focused on the development of a proof-of-concept MIP sensor to detect low concentration of glucose in physiological media, there are still a lot of gaps.

- Use of other recognition moieties: the sandwich-type MIP sensors could offer a huge potential in sensing a variety of catalysts and glucose binding moieties such as: Fe_3O_4, SnO_2 and lectin proteins.
- Investigating selectivity of sandwith-type MIPs: one of the roles of using a MIPs is to differentiate between the molecule of target and other interreferences.

5.3- Contributions

This research offers a facile method to fabricate highly sensitive impedance sensor for glucose sensing with an application in non-invasive or continuous glucose monitoring. The contributions are as follows:

- The potential of using conductive polymers to fabricate impedance sensors. The overoxidized polypyrrole layer provides a suitable conductive layer within the sensor layer that intensifies the senor's impedance performance
- The suggested fabrication of sandwich-type sensor creates criteria for various non-invasive sensing of saccharides such as: fructose, galactose, etc.
- The boronic acid functionalization is proven essential for selective capturing of glucose as opposed to other interfering analytes.
- The accurate optimization of different parameters involving imprinting polymerization step were essential to acquiring high sensitivity for glucose detection.
- This research boasts itself for carefully examining the comparison between MIP and NIP in terms of their electrochemistry and sensitivity toward glucose. NIP did not show variations of charge transfer change while MIP showed noticeable change in charge transfer with different concentrations of glucose.

- Low LOD and LOQ were obtained for MIP based impedimetric sensor which reveals potential for future investigations of this method.

6. Bibliography

1. *Introduction: Standards of Medical Care in Diabetes—2018.* Diabetes Care, 2017. **41**(Supplement_1): p. S1-S2.
2. Lee, H., et al., *Enzyme-Based Glucose Sensor: From Invasive to Wearable Device.* 2018. **7**(8): p. 1701150.
3. Guo, C.X. and C.M. Li, *Direct electron transfer of glucose oxidase and biosensing of glucose on hollow sphere-nanostructured conducting polymer/metal oxide composite.* Physical Chemistry Chemical Physics, 2010. **12**(38): p. 12153-12159.
4. Saha, T., et al., *Wearable Electrochemical Glucose Sensors in Diabetes Management: A Comprehensive Review.* Chemical Reviews, 2023. **123**(12): p. 7854-7889.
5. Zaidi, S.A. and J.H.J.T. Shin, *Recent developments in nanostructure based electrochemical glucose sensors.* 2016. **149**: p. 30-42.
6. Lee, J., et al., *A study on the stability and sensitivity of mediator-based enzymatic glucose sensor measured by catalyst consisting of multilayer stacked via layer-by-layer.* 2021. **93**: p. 383-387.
7. Pickup, J.C., G.W. Shaw, and D.J.J.B. Claremont, *Potentially-implantable, amperometric glucose sensors with mediated electron transfer: improving the operating stability.* 1989. **4**(2): p. 109-119.
8. Abdullahi, S., et al., *Enhancing the sensitivity and accuracy of wearable glucose biosensors: A systematic review on the prospects of mutarotase.* 2024: p. 100231.
9. Caldara, M., et al., *Recent Advances in Molecularly Imprinted Polymers for Glucose Monitoring: From Fundamental Research to Commercial Application.* 2023. **11**(1): p. 32.
10. Wackerlig, J., P.A.J.S. Lieberzeit, and A.B. Chemical, *Molecularly imprinted polymer nanoparticles in chemical sensing–Synthesis, characterisation and application.* 2015. **207**: p. 144-157.
11. BelBruno, J.J.J.C.r., *Molecularly imprinted polymers.* 2018. **119**(1): p. 94-119.
12. Tarasov, S.E., et al., *Impedancemetric Detection of Glucose Using a Biosensor Based on Screen-Printed Electrodes.* Protection of Metals and Physical Chemistry of Surfaces, 2018. **54**(6): p. 1217-1220.
13. Fatke, B., H. Förstl, and A.J.D.D. Risse, *Diabetes.* 2013. **9**: p. 475-486.
14. Coster, S., et al., *Monitoring blood glucose control in diabetes mellitus: a systematic review.* 2000. **4 12**: p. i-iv, 1-93.
15. Alberti, K.G. and P.Z. Zimmet, *Definition, diagnosis and classification of diabetes mellitus and its complications. Part 1: diagnosis and classification of diabetes mellitus provisional report of a WHO consultation.* Diabet Med, 1998. **15**(7): p. 539-53.
16. Organization, W.H., *Noncommunicable diseases in the South-East Asia Region, 2011: situation and response.* 2012.
17. Ernst, S., et al., *The electrooxidation of glucose in phosphate buffer solutions: Part I. Reactivity and kinetics below 350 mV/RHE.* 1979. **100**(1-2): p. 173-183.
18. Waffo, A.F.T., et al., *Fully electrochemical MIP sensor for artemisinin.* Sensors and Actuators B: Chemical, 2018. **275**: p. 163-173.
19. Stojanovic, Z., et al., *Electrosynthesized molecularly imprinted polyscopoletin nanofilms for human serum albumin detection.* 2017. **977**: p. 1-9.
20. Clark Jr., L.C. and C. Lyons, *ELECTRODE SYSTEMS FOR CONTINUOUS MONITORING IN CARDIOVASCULAR SURGERY.* 1962. **102**(1): p. 29-45.

21. Ferri, S., K. Kojima, and K. Sode, *Review of glucose oxidases and glucose dehydrogenases: a bird's eye view of glucose sensing enzymes.* J Diabetes Sci Technol, 2011. **5**(5): p. 1068-76.
22. Wilson, R. and A.P.F. Turner. *Review article Glucose oxidase: an ideal enzyme*. 1992.
23. Suzuki, T., et al., *"Type 1 on type 2" diabetes mellitus: Autoimmune type 1 diabetes superimposed on established type 2 diabetes.* Internal Medicine, 2007. **46**(24): p. 1957-1962.
24. Zhu, H., et al., *Advances in non-enzymatic glucose sensors based on metal oxides.* Journal of Materials Chemistry B, 2016. **4**(46): p. 7333-7349.
25. Largeaud, F., et al., *On the electrochemical reactivity of anomers: electrocatalytic oxidation of α- and β-d-glucose on platinum electrodes in acid and basic media.* 1995. **397**: p. 261-269.
26. Lewis, B.E., et al., *Transition states for glucopyranose interconversion.* J Am Chem Soc, 2006. **128**(15): p. 5049-58.
27. Klimov, E. and H.W. Siesler, *Fourier transform infrared spectroscopic investigation of the electric-field-induced reorientation of the nematic 7CPB with different prealignment.* Appl Spectrosc, 2004. **58**(8): p. 952-7.
28. Clark Jr, L.C., *Membrane polarographic electrode system and method with electrochemical compensation*. 1970, Google Patents.
29. Updike, S.J. and G.P. Hicks, *The enzyme electrode.* Nature, 1967. **214**(5092): p. 986-988.
30. Guilbault, G. and G. Lubrano, *An enzyme electrode for the amperometric determination of glucose.* Analytica chimica acta, 1973. **64**(3): p. 439-455.
31. Moggia, G., et al., *Electrochemical oxidation of d-glucose in alkaline medium: Impact of oxidation potential and chemical side reactions on the selectivity to d-gluconic and d-glucaric acid.* ChemElectroChem, 2020. **7**(1): p. 86-95.
32. Tsai, Y.-C., S.-C. Li, and S.-W. Liao, *Electrodeposition of polypyrrole–multiwalled carbon nanotube–glucose oxidase nanobiocomposite film for the detection of glucose.* Biosensors and Bioelectronics, 2006. **22**(4): p. 495-500.
33. Toghill, K.E. and R.G. Compton, *Electrochemical Non-enzymatic Glucose Sensors: A Perspective and an Evaluation.* International Journal of Electrochemical Science, 2010. **5**(9): p. 1246-1301.
34. de Mele, M.F.L., H.A. Videla, and A.J. Arvía, *Potentiodynamic Study of Glucose Electro-Oxidation at Bright Platinum Electrodes.* Journal of The Electrochemical Society, 1982. **129**(10): p. 2207.
35. Vassilyev, Y.B., O.A. Khazova, and N.N.J.J.o.E.C. Nikolaeva, *Kinetics and mechanism of glucose electrooxidation on different electrode-catalysts: Part I. Adsorption and oxidation on platinum.* 1985. **196**: p. 105-125.
36. Popović, K.D., et al., *Structural effects in electrocatalysis: Oxidation of D-glucose on single crystal platinum electrodes in alkaline solution.* 1991. **313**: p. 181-199.
37. O'Mullane, A.P., et al., *Premonolayer oxidation of nanostructured gold: an important factor influencing electrocatalytic activity.* Langmuir, 2009. **25**(6): p. 3845-52.
38. Ducrocq, C., et al., *[Intervention by nitric oxide, NO, and its oxide derivatives particularly in mammals].* Can J Physiol Pharmacol, 2001. **79**(2): p. 95-102.
39. Medway, S.L., et al., *In situ studies of the oxidation of nickel electrodes in alkaline solution.* Journal of Electroanalytical Chemistry, 2006. **587**: p. 172-181.

40. Schouten, K.J.P., E. Pérez-Gallent, and M. Koper, *The electrochemical characterization of copper single-crystal electrodes in alkaline media.* Journal of Electroanalytical Chemistry, 2013. **699**: p. 6–9.
41. Cui, X., L. Hong, and X. Lin, *Electrocatalytic oxidation of hydroxylamine on glassy carbon electrodes modified by hybrid copper-cobalt hexacyanoferrate films.* Anal Sci, 2002. **18**(5): p. 543-7.
42. Choi, S.J., B.G. Choi, and S.M. Park, *Electrochemical sensor for electrochemically inactive beta-D(+)-glucose using alpha-cyclodextrin template molecules.* Anal Chem, 2002. **74**(9): p. 1998-2002.
43. Shoji, E. and M.S. Freund, *Potentiometric sensors based on the inductive effect on the pK(a) of poly(aniline): a nonenzymatic glucose sensor.* J Am Chem Soc, 2001. **123**(14): p. 3383-4.
44. Cheng, Z., E. Wang, and X. Yang, *Capacitive detection of glucose using molecularly imprinted polymers.* Biosens Bioelectron, 2001. **16**(3): p. 179-85.
45. Wu, X., et al., *Selective sensing of saccharides using simple boronic acids and their aggregates.* Chemical Society Reviews, 2013. **42**(20): p. 8032-8048.
46. Egawa, Y., R. Miki, and T. Seki, *Colorimetric Sugar Sensing Using Boronic Acid-Substituted Azobenzenes.* 2014. **7**(2): p. 1201-1220.
47. Çiftçi, H., et al., *Non-enzymatic sensing of glucose using a glassy carbon electrode modified with gold nanoparticles coated with polyethyleneimine and 3-aminophenylboronic acid.* 2016. **183**: p. 1479-1486.
48. Tretjakov, A., et al., *Surface molecularly imprinted polydopamine films for recognition of immunoglobulin G.* Microchimica Acta, 2013. **180**(15): p. 1433-1442.
49. Wang, Q., et al., *Sensitive sugar detection using 4-aminophenylboronic acid modified graphene.* Biosens Bioelectron, 2013. **50**: p. 331-7.
50. Haupt, K. and K. Mosbach, *Molecularly imprinted polymers and their use in biomimetic sensors.* Chem Rev, 2000. **100**(7): p. 2495-504.
51. Das, D., et al., *A Glucose Sensor Based on an Aminophenyl Boronic Acid Bonded Conducting Polymer.* Electroanalysis, 2011. **23**.
52. Maier, N.M. and W. Lindner, *Chiral recognition applications of molecularly imprinted polymers: a critical review.* Anal Bioanal Chem, 2007. **389**(2): p. 377-97.
53. Hansen, J., et al., *Arylboronic acids: A diabetic eye on glucose sensing.* Sensors and Actuators B: Chemical, 2012. **161**: p. 45–79.
54. Dąbrowski, M., et al., *Facile Fabrication of Surface-Imprinted Macroporous Films for Chemosensing of Human Chorionic Gonadotropin Hormone.* ACS Applied Materials & Interfaces, 2019. **11**(9): p. 9265-9276.
55. Iskierko, Z., et al., *Molecularly imprinted polymers for separating and sensing of macromolecular compounds and microorganisms.* Biotechnology Advances, 2016. **34**(1): p. 30-46.
56. Deore, B. and M.S. Freund, *Saccharide imprinting of poly(aniline boronic acid) in the presence of fluoride.* Analyst, 2003. **128**(6): p. 803-806.
57. Zhang, J., et al., *Electrochemical preparation of surface molecularly imprinted poly(3-aminophenylboronic acid)/MWCNTs nanocomposite for sensitive sensing of epinephrine.* Materials Science and Engineering: C, 2018. **91**: p. 696-704.
58. Hallemans, N., et al., *Electrochemical impedance spectroscopy beyond linearity and stationarity—A critical review.* Electrochimica Acta, 2023. **466**: p. 142939.

59. Dai, Y. and C.C. Liu, *A Simple, Cost-Effective Sensor for Detecting Lead Ions in Water Using Under-Potential Deposited Bismuth Sub-Layer with Differential Pulse Voltammetry (DPV) %M doi:10.3390/s17050950 %U https://www.mdpi.com/1424-8220/17/5/950*. Sensors %@ 1424-8220, 2017. **17**(5): p. 950.
60. Galeotti, M., *Electrochemical impedance spectroscopy (EIS) techniques for the evaluation of the state of health (SOH) of batteries.* 2014.
61. Lynk, T.P., *Development of an electrochemical-surface enhanced Raman spectroscopic (EC-SERS) sensor for bacterial screening.* 2018.
62. Rychagov, A.Y. and Y.M. Volfkovich, *Interaction of activated carbon electrodes with sulfuric acid solutions.* Russian Journal of Electrochemistry, 2007. **43**(11): p. 1273-1278.
63. Colin, C., et al., *Easy cleaning plus stable activation of glassy carbon electrode surface by oxygen plasma.* Bioelectrochemistry, 2023. **154**: p. 108551.
64. Atchabarova, A., et al., *Electrochemical modification of the carbon material surface by hydroxyl groups.* Journal of Solid State Electrochemistry, 2024. **28**(7): p. 2425-2436.
65. Sadki, S., et al., *The mechanisms of pyrrole electropolymerization.* Chemical Society Reviews, 2000. **29**(5): p. 283-293.
66. Ramanavičius, A., A. Ramanavičienė, and A. Malinauskas, *Electrochemical sensors based on conducting polymer—polypyrrole.* Electrochimica acta, 2006. **51**(27): p. 6025-6037.
67. Andreev, E.A., et al., *Reagentless Impedimetric Sensors Based on Aminophenylboronic Acids.* Journal of Analytical Chemistry, 2019. **74**(2): p. 153-171.
68. Lacina, K., P. Skládal, and T.D. James, *Boronic acids for sensing and other applications - a mini-review of papers published in 2013.* Chemistry Central Journal, 2014. **8**(1): p. 60.
69. Wang, H.-C., et al., *A bis-boronic acid modified electrode for the sensitive and selective determination of glucose concentrations.* Analyst, 2013. **138**(23): p. 7146-7151.
70. Wu, H., et al., *Non-enzymatic glucose sensor based on molecularly imprinted polymer: a theoretical, strategy fabrication and application.* Journal of Solid State Electrochemistry, 2019. **23**(5): p. 1379-1388.
71. Shan, H., et al., *Facile access to highly flexible and mesoporous structured silica fibrous membranes for tetracyclines removal.* Chemical Engineering Journal, 2021. **417**: p. 129211.
72. Qian, R., J. Qiu, and D. Shen, *Conducting polypyrrole electrochemically prepared from aqueous solutions.* Synthetic Metals, 1987. **18**(1-3): p. 13-18.
73. Lin, J., et al., *Research trends in electrospun conducting polymers derived CNFs and their composite as the potential electrodes for high-performance flexible supercapacitors.* Journal of Energy Storage, 2024. **96**: p. 112605.
74. Bachhav, S.G. and D.R. Patil, *Study of polypyrrole-coated MWCNT nanocomposites for ammonia sensing at room temperature.* Journal of Materials Science and Chemical Engineering, 2015. **3**(10): p. 30-44.
75. Huang, L., et al., *Electrochemical sensor based on molecularly imprinted polypyrrole-MWCNTs-OH/covalent organic framework for the detection of ofloxacin in water.* Microchimica Acta, 2024. **192**(1): p. 3.
76. Rashed, M.A., et al., *MWCNT-doped polypyrrole-carbon black modified glassy carbon electrode for efficient electrochemical sensing of nitrite ions.* Electrocatalysis, 2021. **12**: p. 650-666.

77. Arulraj, A.D., et al., *Polypyrrole with a functionalized multi-walled carbon nanotube hybrid nanocomposite: a new and efficient nitrite sensor.* New Journal of Chemistry, 2018. **42**(5): p. 3748-3757.
78. Farbod, M., E. Elahi asl, and S.S. Shojaeenezhad, *Polypyrrole/multi-walled carbon nanotube nanocomposite as a high-performance material for supercapacitors' electrodes.* Journal of Applied Electrochemistry, 2023. **53**(8): p. 1623-1630.
79. Singh, K., et al., *Fabrication of amperometric bienzymatic glucose biosensor based on MWCNT tube and polypyrrole multilayered nanocomposite.* Journal of Applied Polymer Science, 2012. **125**(S1): p. E235-E246.
80. Ma, Q., et al., *Bioresponsive functional phenylboronic acid-based delivery system as an emerging platform for diabetic therapy.* International Journal of Nanomedicine, 2021: p. 297-314.
81. Liu, L., et al., *Boronic acid-based electrochemical sensors for detection of biomolecules.* International Journal of Electrochemical Science, 2013. **8**(9): p. 11161-11174.
82. He, J.-Y., et al., *Specific capture and determination of glycoprotein using a hybrid epitopes and monomers-mediated molecular-imprinted polymer enzyme-free electrochemical biosensor.* Microchimica Acta, 2023. **190**(4): p. 118.
83. Sorrell, C.D. and M.J. Serpe, *Glucose sensitive poly (N-isopropylacrylamide) microgel based etalons.* Analytical and Bioanalytical Chemistry, 2012. **402**(7): p. 2385-2393.
84. Liu, L., et al., *Biosensors with Boronic Acid-Based Materials as the Recognition Elements and Signal Labels.* Biosensors, 2023. **13**(8): p. 785.
85. Xia, X., et al., *Intrinsically electron conductive, antibacterial, and anti-swelling hydrogels as implantable sensors for bioelectronics.* Advanced Functional Materials, 2022. **32**(48): p. 2208024.
86. Inzelt, G., *Conducting polymers: a new era in electrochemistry*. 2012: Springer Science & Business Media.
87. Li, Y., et al., *Recent advances in molecularly imprinted polymer-based electrochemical sensors.* Biosensors and Bioelectronics, 2024. **249**: p. 116018.
88. Caldara, M., et al., *Recent Advances in Molecularly Imprinted Polymers for Glucose Monitoring: From Fundamental Research to Commercial Application.* Chemosensors, 2023. **11**(1): p. 32.
89. Zidarič, T., et al., *The development of an electropolymerized, molecularly imprinted polymer (MIP) sensor for insulin determination using single-drop analysis.* Analyst, 2023. **148**(5): p. 1102-1115.
90. Sęk, J.P., et al., *Boronate-appended polymers with diol-functionalized ferrocene: an effective and selective method for voltammetric glucose sensing.* Dalton Transactions, 2021. **50**(3): p. 880-889.
91. Mašković, S. and N. Nikolac Gabaj, *Ascorbic acid and glucose can cause significant interference on quantitative measurement of biochemistry analytes in urine.* Laboratory Medicine, 2024: p. lmae089.
92. Zhong, X., et al., *A Reusable Interface Constructed by 3-Aminophenylboronic Acid-Functionalized Multiwalled Carbon Nanotubes for Cell Capture, Release, and Cytosensing.* Advanced Functional Materials, 2010. **20**(6): p. 992-999.
93. Caldara, M., et al., *Thermal Detection of Glucose in Urine Using a Molecularly Imprinted Polymer as a Recognition Element.* ACS Sensors, 2021. **6**(12): p. 4515-4525.

94. Wu, Y., et al., *An Enzyme Free Potentiometric Detection of Reducing Sugars Based on a Poly(3-hydroxyphenylboronic acid-co-phenol) Molecularly Imprinted Polymer Modified Electrode.* American Journal of Biomedical Sciences, 2016: p. 82-96.
95. Cho, S.J., et al., *A selective glucose sensor based on direct oxidation on a bimetal catalyst with a molecular imprinted polymer.* Biosensors & Bioelectronics, 2018. **99**: p. 471-478.
96. Yang, Y., et al., *Glucose sensors based on electrodeposition of molecularly imprinted polymeric micelles: A novel strategy for MIP sensors.* Biosensors and Bioelectronics, 2011. **26**(5): p. 2607-2612.